

Model Utility Law: Evaluating LLMs beyond Performance through Mechanism Interpretable Metric

Yixin Cao^{1*} Jiahao Ying² Yaoning Wang¹ Xipeng Qiu¹ Xuanjing Huang¹ Yugang Jiang¹

¹School of Computer Science, Fudan University

²School of Computer Science, Singapore Management University

yxcao@fudan.edu.cn jhying.2022@phdcs.smu.edu.sg

Abstract

Large Language Models (LLMs) have become indispensable across academia, industry, and daily applications, yet current evaluation methods struggle to keep pace with their rapid development. One core challenge of evaluation in the large language model (LLM) era is the generalization issue: how to infer a model’s near-unbounded abilities from inevitably bounded benchmarks. We address this challenge by proposing Model Utilization Index (MUI), a mechanism interpretability enhanced metric that complements traditional performance scores. MUI quantifies the effort a model expends on a task, defined as the proportion of activated neurons or features during inference. Intuitively, a truly capable model should achieve higher performance with lower effort. Extensive experiments across popular LLMs reveal a consistent inverse logarithmic relationship between MUI and performance, which we formulate as the Utility Law. From this law we derive four practical corollaries that (i) guide training diagnostics, (ii) expose data contamination issue, (iii) enable fairer model comparisons, and (iv) design model-specific dataset diversity².

1 Introduction

Recent years have witnessed an explosion of research interest in evaluating large language models (LLMs). Rigorous evaluation not only identify model weaknesses to guide optimization but also helps to define new objectives for next-generation models. Although many benchmarks have emerged, researchers have highlighted a generalization issue in evaluation [6]. With increasing data, compute, and parameters, LLMs’ capabilities can scale nearly without bound (i.e., scaling law), but the size of benchmarks remains bounded due to practical efficiency concerns. Consequently, a key challenge in the era of LLMs lies in estimating a model’s true performance and potential beyond what is explicitly reflected in limited testing samples.

In this paper, we propose a new metric, Model Utilization Index (MUI), for generalizable evaluation. The basic idea parallels human assessment: when judging an individual, we weigh not only what they achieve but also how much effort they expend. MUI targets the latter dimension for LLMs, complementary to conventional performance metrics. Clearly, the underlying assumption is that the less effort required to achieve a better result (i.e., lower MUI and higher performance score), the stronger the model’s true ability. However, how to quantify the model’s effort?

Inspired by recent advances in mechanistic interpretability, we define MUI as the measurement of the degree to which a model utilizes its capabilities during inference, calculated by the proportion of neurons or features activated to complete given tasks. In this field it is regarded that all of the model abilities, once it has been thoroughly trained, are encoded in neurons or in distinctive activation

*Corresponding authors.

²Our code can be found at <https://github.com/ALEX-nlp/MUI-Eval>

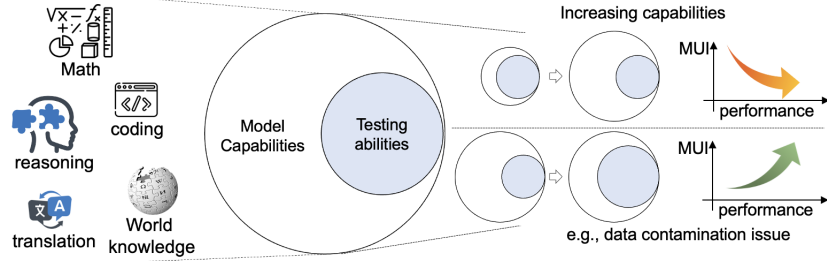


Figure 1: Illustration of model utility: how much effort (i.e., activated abilities) utilized to complete given tasks. Two example cases for generalizable evaluation: 1) A more capable model should achieve higher performance with less effort (lower MUI). 2) When data contamination occurs, higher performance is achieved by utilizing more effort (higher MUI), while model’s overall capabilities remain unchanged or even weakened.

patterns across them. Neuron-level studies support this premise by showing that specific concepts are consistently localized [28]. When the model produces a given concept, the same subset of neurons contributes far more than the rest, responsible for utilizing that capability. Similarly, instead of localizing neurons, another line of works like sparse auto-encoders (SAEs) explains the model behaviors by mapping neuron activation patterns into a sparse feature space [20]. When the model expresses a particular skill, only a handful of features being activated. Thus, as illustrated in Figure 1, compared with a model’s overall capabilities, solving given tasks only utilizes a fraction of its neurons or features (the inner highlighted circle). Our MUI quantifies this ratio as the measurement of the model effort.

By integrating MUI with performance metrics, we achieve a generalizable evaluation that transcends the limitations of bounded benchmarks, thereby alleviating various related assessment issues. We have conducted a series of experiments for verification. The insights are summarized as follows:

- **Model Utility Law.** Agree with our assumption, MUI exhibits a negative logarithm relationship with performance. This also explains why sparse mixture-of-expert (MoE) model performs better – it is not merely because of larger-scale parameters, but the introduction of an additional optimization objective to lower model utility. Our law suggests a limit sparsity ratio (Section 3.2).
- **Corollary 1 for training diagnostics.** An increase in MUI may signal potential degradation of unseen capabilities. We conclude four optimization directions based on MUI and performance curve for deeply analyzing the training process using a limited set of testing samples (Section 3.3).
- **Corollary 2 for data contamination analysis.** Unlike standard pre-training or post-training, contamination inflates performance with increasing MUI, accompanied by a specific optimization trajectory (Section 3.4).
- **Corollary 3 for fair model comparison.** More capable model should be indicated by both higher performance and lower MUI. This also explains why two models with similar leaderboard scores can differ markedly in user experience; higher MUI reveals those that rely on brute utilisation rather than enhanced fundamental capability (Section 3.5).
- **Corollary 4 for data diversity.** For a fixed model, optimal data variety should elicit maximal breadth of a model’s capacities, a.k.a., higher MUI. Compared to traditional data diversity measurements like domains and capabilities, MUI is not only a comprehensive indicator, but it also emphasizes that diversity is model-specific (Section 3.6).

Of course, MUI is still limited by the current state of interpretability techniques, whose progress will continuously push forward a more precise model utilization evaluation.

2 New Metric: Model Utilization Index

In this section, we define model utilization for LLMs, aiming to assess how much effort a model expends to achieve a given outcome. This allows us to use it as a complement to performance metrics, providing an estimate of the model’s overall capabilities through a limited test set, or conversely, tailored to benchmark dataset curation, making the evaluation fairer and more comprehensive. Next, we first briefly describe several typical interpretability techniques, following by the definition of our proposed Model Utilization Index (MUI).

2.1 Preliminary

Recent advancements in understanding LLMs have increasingly highlighted the importance of mechanistic interpretability [15, 35, 26, 11, 5], a method that aims to reverse-engineer these complex models at a more granular level. This approach goes beyond black-box testing by examining the inner workings of neural networks—investigating how individual components, such as neurons and layers, interact to produce the model’s overall behavior. The goal is to uncover the causal mechanisms that drive the model’s responses, offering a deeper understanding of its decision-making processes. Before introducing our proposed metric, we will briefly explore two prominent techniques in mechanistic interpretability: neuron-based and Sparse Activation Encoding (SAE) based Interpretability.

2.1.1 Neuron-Based Interpretability

Neuron-level [12, 35, 18] interpretable methods connect individual neurons in the Feed-forward network (FFN) sub-layer of LLMs to specific semantic meanings. These neurons are treated as mediator variables [26] for certain model behaviors. A causal relationship between model behaviors and neuron activations is constructed by intervention techniques, such as neuron activation patching [34, 26, 7], neuron activation comparison [35], and neuron gradient comparison [12]. As a large portion of neurons are shown to be connected to certain interpretable concepts [4], we use their activation footprints to measure model utilization.

Considering the large number of neurons within LLMs, before testing the causal effect, the most important step in neuron-level analyses is identifying key neurons that are activated and functioning for a certain task of interest, i.e., the actually utilized neurons in the model for performing the task. The most common pipeline for identifying key neurons is to calculate a contribution score for each neuron quantifying the contribution of the neuron to solving the task and then setting up a threshold to select the key neurons with scores over the threshold. There are various ways to calculate the contribution score, such as using gradient-based attribution [12], correlations to prediction [35], and contribution to certain tokens [28, 15, 16]. In our implementation, we follow a straightforward but effective way of defining the contribution score of a neuron as its contribution to promoting the prediction of the desired output token at the position of the last token before prediction [28, 15, 16].

Specifically, omitting the layer normalization for the sake of brevity, the FFN sub-layer of layer l can be considered as the function:

$$\text{FFN}^l(\mathbf{x}) = \mathbf{W}_{\text{out}}^l \sigma(\mathbf{W}_{\text{in}}^l(\mathbf{x})), \quad (1)$$

where σ is an activation function, \mathbf{W}_{in}^l and $\mathbf{W}_{\text{out}}^l$ are the first/second linear layer in FFN. The contribution score of the i -th neuron in layer l for prediction token \hat{y} given input x can be defined as:

$$f_{\text{neuron}}(i, l, \hat{y} | x) = \left(\mathbf{W}_u \mathbf{W}_{\text{out}}^l \circ \sigma(\mathbf{W}_{\text{in}}^l(\mathbf{x}_{-1}^l)) \right)_{i, \hat{y}}, \quad (2)$$

where \mathbf{W}_u is the unembedding matrix transforming the hidden states into scores over the vocabulary, \circ is an element-wise product with broadcasting, and \mathbf{x}_{-1}^l denotes the input of FFN in the last token before predicting \hat{y} at l -th layer. Consider a task sample $t = (x, y)$ from the evaluation dataset $T = \{(x_1, y_1), (x_2, y_2), \dots, (x_{|T|}, y_{|T|})\}$. For a given threshold η , the key neurons for task sample t is defined as:

$$N_{\text{neuron}}(t) = \left\{ (i, l) \mid f_{\text{neuron}}(i, l, \hat{y}_j | x + \hat{y}_{<j}) > \eta, \hat{y}_j \in y, l \in \{1, 2, \dots, L\}, i \in \{1, 2, \dots, N\} \right\}, \quad (3)$$

where: $\hat{y}_{<j} = (\hat{y}_1, \hat{y}_2, \dots, \hat{y}_{j-1})$ denotes the partial response sequence before the j -th token \hat{y}_j , L represents the total number of layers in the model, and N indicates the number of neurons per layer. These key neurons represent the essential components to produce the output y given x . In other words, they reflect the “effort” the model exerts to achieve the response.

2.1.2 SAE-based Interpretability

Sparse-Autoencoder (SAE) is similar to neuron analysis but is proposed to offer clearer insights into what information the LLM is processing. By learning a sparse representation of neural activations [24,

20], the SAE effectively segregates overlapping concepts or features into distinct, interpretable feature or concept units, thereby addressing the challenge of *polysemanticity* in neuron-level interpretation. Specifically, SAEs project the hidden states from the l^{th} layer of an LLM, denoted as \mathbf{x}^l , into a high-dimensional feature space using a linear encoder parameterized by matrix \mathbf{W}_e^l . A corresponding decoder, defined by \mathbf{W}_d^l , reconstructs the original hidden states. To promote sparsity in the extracted features, the encoder’s output undergoes post-processing with a sparsity-enforcing constraint (e.g., TopK [14, 20], JumpReLU [24]), which limits the number of non-zero values in the output, thus ensuring that only input corresponding features are retained.

$$\mathbf{f}^l = \text{SparsityConstraint}(\mathbf{W}_e^l \mathbf{x}^l), \quad \mathbf{W}_d^l \mathbf{f}^l \approx \mathbf{x}^l \quad (4)$$

The projected mono-semantic features dictionary $\mathbf{f}^l \in \mathbb{R}^D$ contains D features. We define the score of the i^{th} feature in layer l in relation to its contribution for prediction \hat{y} for a given input \mathbf{x} as follows:

$$f_{\text{sae}}(i, l, \hat{y} \mid \mathbf{x}) = \text{SparsityConstraint}(\mathbf{W}_e^l \mathbf{x}_{-1}^l)_{i, \hat{y}} \quad (5)$$

Similar to neuron analysis, for a given threshold η , the key features for completion task sample t is defined as:

$$N_{\text{sae}}(t) = \left\{ (i, l) \mid f_{\text{sae}}(i, l, \hat{y}_j \mid \mathbf{x} + \hat{y}_{<j}) > \eta, \hat{y}_j \in \mathbf{y}, l \in \{1, 2, \dots, L\}, i \in \{1, 2, \dots, D\} \right\}, \quad (6)$$

2.2 Model Utilization Index

Now, we formally define Model Utilization Index (MUI) as follows:

$$\text{MUI} = \frac{N_{\text{activated}}(T)}{N_{\text{total}}}$$

where N_{total} denotes the total capabilities of the model, $N_{\text{activated}}(T)$ denotes the number of activated capabilities when the model completes the tasks T , e.g., samples in the test set. Now, we define the capabilities through mechanism interpretability techniques.

When we leverage neuron-based methods, the equation is instantiated as:

$$\text{MUI}_{\text{neuron}} = \frac{N_{\text{activated}}(T, \text{neurons})}{N_{\text{total}}(\text{neurons})}$$

$$N_{\text{activated}}(T, \text{neurons}) = \left| \bigcup_{t=1}^T \{i \mid i \in N_{\text{neuron}}(t)\} \right|$$

where $N_{\text{neuron}}(t)$ is defined in Section 2.1.1. In experiments, we pick up Top $k\%$ neurons with highest activation values in each layer to setup the threshold η , to avoid the impacts of model scale.

When we leverage SAE-based methods, MUI is instantiated as:

$$\text{MUI}_{\text{feature}} = \frac{N_{\text{activated}}(T, \text{features})}{N_{\text{total}}(\text{features})}$$

$$N_{\text{activated}}(T, \text{features}) = \left| \bigcup_{t=1}^T \{i \mid i \in N_{\text{sae}}(t)\} \right|$$

where $N_{\text{sae}}(t)$ is defined in Section 2.1.2. In experiments, we pick up Top $k\%$ active features in each SAE layer, to avoid the impacts of the size of pre-defined SAE features.

3 Experiments

3.1 Setup

Dataset Selection. To ensure reliable conclusions, we select diverse and widely used benchmarks. Following [17, 38], we include 1) GSM8K [10] and MATH [22] for math reasoning, 2) HumaEval [8] and MBPP [1] for coding, 3) ARC-Challenge [9] for science (including math) reasoning, and 4) BIG-bench Hard (BBH) [3] and MMLU [21] to cover general tasks. Statistical result for the selected benchmarks is shown in Table 2.

Model Selection. To maximize the applicability of MUI and ensure the fairness of the evaluation, we carefully select four series of widely used open-sourced LLMs: 1) Llama Series including Vicuna-7B-v1.3 [29], Llama-2-7B-Chat [33], Llama-3.1-8B, Llama-3.1-8B-Instruct [17], CodeLlama-7B-Instruct [30] and DeepSeek-R1-Distill-Llama-8B [13], 2) Qwen series including Qwen1.5-7B-Chat [2], Qwen2.5-7B-Instruct [32], Qwen2.5-Coder-7B-Instruct [23], Qwen2.5-Math-7B-Instruct [36] and DeepSeek-R1-Distill-Qwen-7B [13], 3) Gemma series including Gemma-2-9B and Gemma-2-9B-Instruct [31], 4) OLMo series including several checkpoints from OLMo-2-7B [27] (detailed checkpoints information is shown in Appendix A.2). Note that we select merely ~7B LLMs considering the cost and those models are more probably trained well. Nevertheless, we also include some larger models in Table 5 for exploratory analysis, where the results are basically consistent with our claims. More details for neuron-based and SAE-based method setup can be found in Appendix.

3.2 Utility Law

Utility Law. Inverse Relationship Between Capability and MUI: As foundational capability increases, model utilization on a fixed dataset decreases.

We first verify MUI by introducing a common phenomenon that is consistent with our hypothesis: the less effort required to achieve a better result, the stronger the individual’s ability. We selected several fundamental LLMs, excluding those specifically optimized, such as CodeLlama, which will be analyzed later. By fitting the relationship between MUI and the corresponding performance across various datasets, we observed a universal law as shown in Figure 2 and Figure 3.

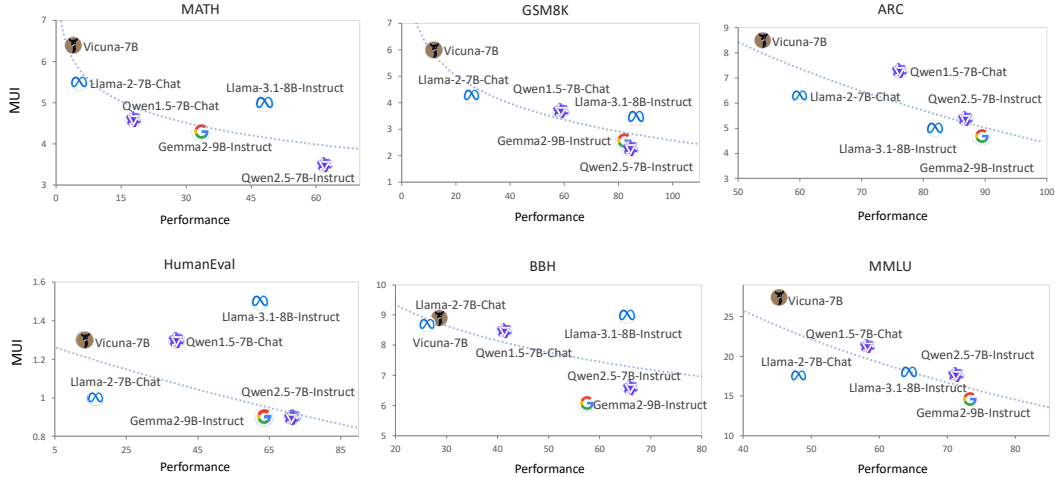


Figure 2: Relationship between performance (accuracy) and neuron-based MUI. The dashed line represents the trend line fitted using a logarithmic function. Due to space limitation, the results of MBPP can be found in Appendix B.1.

Figure 2 illustrates the MUI-performance curve for models on mathematics, coding, and comprehensive datasets, while Figure 3 aggregates all of the aforementioned datasets (excluding MMLU due to its high inference cost). It is important to note that Figure 3 does not represent a simple weighted

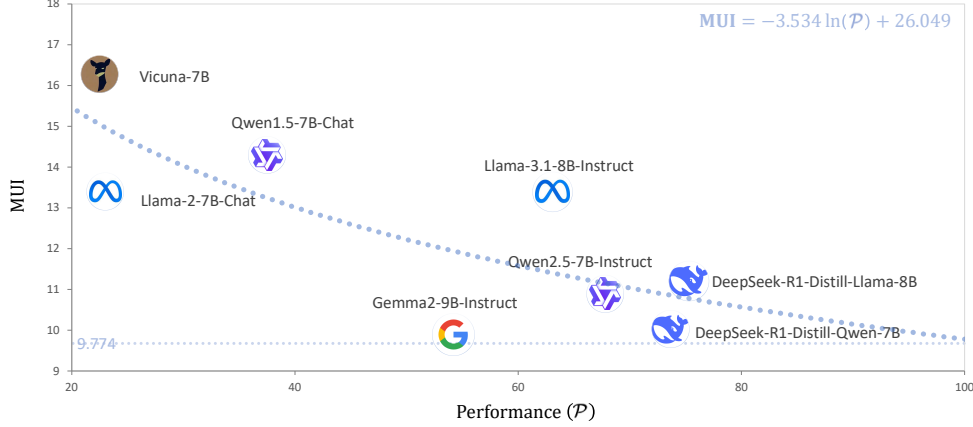


Figure 3: Overall MUI-performance relationship across six datasets. MMLU is excluded due to DeepSeek series model inference cost considerations. According to model utilization curve, when performance reaches 100%, the minimum MUI is around 9.77%.

average across all datasets, as the number of activated neurons in the MUI formula varies with the increasing amount of data. Specifically, we observe that the MUI-performance curve exhibits an approximately negative logarithmic:

$$\text{MUI} = A \ln(\mathcal{P}) + B$$

where \mathcal{P} denotes performance score, and we have $A = -3.534$, $B = 26.049$ for overall relationship. We also observe similar trend using SAE-based MUI, which can be found in Appendix B.1.

From the above model utilization law, we can observe that: 1) From the upper left to the lower right, the ranking of model capabilities generally aligns with expectations. In particular, for models with similar performance, such as Vicuna and Llama2, MUI distinctly differentiates their ability levels. A more detailed analysis is provided in Section 3.5 (Corollary 3); 2) This theorem can also explain why MoE models (e.g., Deepseek R1) perform well, as they incorporate a sparsity objective during optimization, which is equivalent to minimizing MUI; 3) There are two special points on the logarithmic curve. First, as performance approaches zero, MUI tends toward infinity, implying that evaluation loses its meaning; second, when the performance score reaches 100%, MUI approaches approximately 9.77%. This may indicate a limit compression ratio — if a lower MUI is preferable, then this value represents the minimum expected model utilization, thus providing guidance for training. Of course, due to dataset limitations and the constraints of interpretability techniques, this value may not be precise. We will continue to explore this further.

3.3 MUI for Model Training

Corollary 1. Training diagnostics: During model training, an increase in model utilization on some dataset may indicate a decline in other capabilities beyond the dataset.

As mentioned above, in the MUI-performance curve, the progression from the upper left to the lower right represents an improvement in the model’s fundamental capability: lower MUI coupled with higher performance. Inspired by this, we further explore the other directions to analyze the training process of a model for regression testing. As shown in Figure 4, we first define four optimization directions: 1) **Evolving**: The model demonstrates improved performance with a smaller MUI, indicating genuinely enhanced capability. 2) **Accumulating**: The model shows better performance but with an increased MUI, which may suggest that a particular ability has been emphasized or seemingly improved. 3) **Coarsening**:

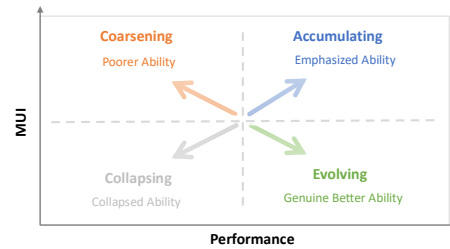


Figure 4: Optimization directions: evolving, accumulating, coarsening, and collapsing.

The model exhibits poorer performance with an increased MUI, indicating reduced abilities on this task. 4) **Collapsing**: The model displays poorer performance with a smaller MUI, suggesting a comprehensive breakdown in model functionality.

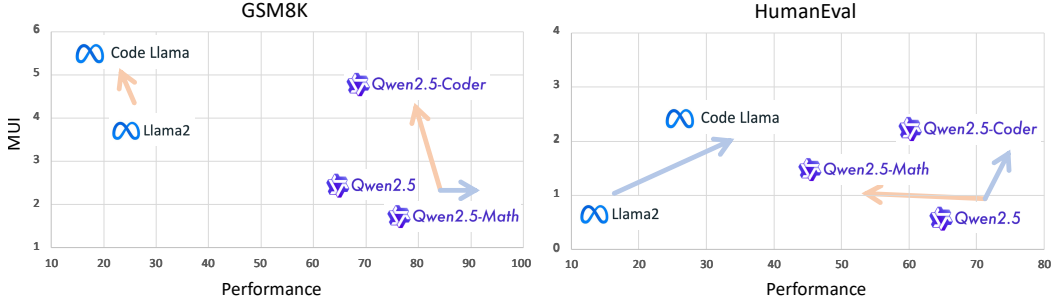


Figure 5: MUI and Performance relationship, studied on Llama / Qwen series. We basically compare the math / code versions with the base models, to see the changes using in-domain testing and out-of-domain testing (e.g., for code version, HumanEval is in-domain and GSM8K is out-of-domain). The orange arrow from the right lower side to the left upper side denotes the coarsening direction, and the blue arrow from the left lower side to right upper side denotes the accumulating direction.

We now empirically demonstrate these four directions based on existing LLMs, followed by investigating the pre-training progress of the OLMo series thanks to its open-source details. First, for the evolving direction, we have demonstrated it in Section 3.2. Similar trend can also be found in Figure 14, if we only include the same series of LLMs, e.g., vicuna, Llama2, Llama3.1, and Deepseek-distill-Llama. Second, for the coarsening and accumulating directions, we assume that these two typically occur during the process of enhancing specific abilities. We thus choose math reasoning and coding as two types of enhanced abilities, observing the Llama series: Llama-2-7B-Chat and CodeLlama-7B-Instruct, where the latter is tuned on coding data based on the former LLM, and the Qwen series: Qwen2.5-7B-Instruct and its coding/math optimized versions, Qwen2.5-Coder-7B-Instruct and Qwen2.5-Math-7B-Instruct. As shown in Figure 5, we can see that the specialized versions move in the accumulating direction compared with the base model if testing on the datasets for targeted abilities, e.g., CodeLlama vs Llama2 on HumanEval, Qwen2.5-Coder vs Qwen2.5 on HumanEval, and Qwen2.5-Math vs Qwen2.5 on GSM8k, while the specialized versions move in the coarsening direction compared with the base model if testing on the out-of-domain (OOD) benchmark, e.g., CodeLlama vs Llama2 on GSM8k, Qwen2.5-Coder vs Qwen2.5 on GSM8k, and Qwen2.5-Math vs Qwen2.5 on HumanEval. We attribute the main reason is when the performance improvement on a particular task has not yet reached the level of fundamental capability enhancement—primarily due to an overall distributional shift towards that ability—it corresponds to the accumulating direction (with an increase in MUI and performance). Simultaneously, this shift results in decreased performance on other tasks, characterizing the coarsening direction (with an increase in MUI and a decrease in performance). Full results on the selected tasks shown in Table 5 and Table 9. This observation in turn suggests that using MUI as an indicator on one fixed dataset can relate to changes in other capabilities, which we summarize as Corollary 1. Third, for the collapsing direction, we only observe it when data contamination occurs, which will be detailed in Section 3.4.

Now, to investigate the changes during pre-training, we select a series of checkpoints of OLMo-2-7B, ranging from training with 0.5T of data up to 4T. As shown in Figure 6, there are similar curves when testing using different datasets. Here we present MATH and BBH, and full results are presented in Figure 15 and Table 8. We can see that the model initially exhibits an accumulating direction, progressing until the final 200k steps (3T to 4T), whereas evolving trend becomes uniformly evident. Additionally, by investigating fine-grained intermediate steps in the accumulating direction, as shown in Figure 7, we observe it accompanied by both coarsening and evolving trends on different evaluation tasks, which indicates different capabilities being enhanced separately, eventually leading to a comprehensive enhancement—the evolving direction. By closely monitoring changes in MUI on limited datasets, we can identify overall trends in model capabilities improvement and make timely, targeted adjustments. We thus summarize it as Corollary 1 beneficial for training guidance.

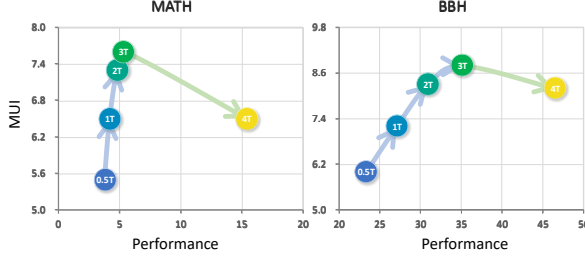


Figure 6: MUI-Performance curve for OLMo-2-7B trained using 0.5T, 1T, 2T, 3T, 4T tokens on MATH and BBH.

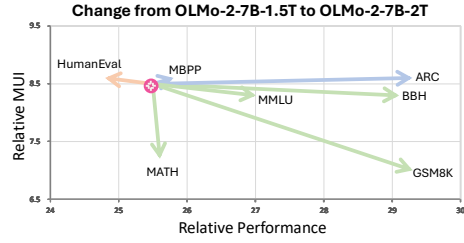


Figure 7: Illustration of relative MUI-Performance curve for OLMo-2-7B trained using 1.5T and 2T data across seven tasks.

3.4 MUI for Data Contamination

Corollary 2. Data Contamination Detection: *When a model achieves inflated performance through data contamination, it does not reduce model utilization; instead, utilization increases as other capabilities are compromised.*

In the previous section, we showed that optimizing a model for a single capability drives its MUI-performance curve along the coarsening and accumulating directions. Here, we examine how the curve changes under data contamination. To simulate this issue, we fine-tuned three models: Llama-2-7B-Chat, Llama-3.1-8B-Instruct, and Qwen-2.5-7B-Instruct, using the test samples of GSM8K and MATH following [37], detailed hyper-parameters are listed in Appendix A.6. The results are shown in Figure 8, and full results with similar trends appear in Table 10.

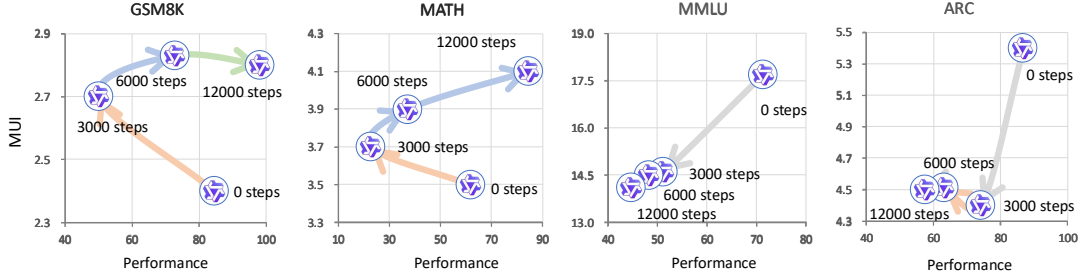


Figure 8: Simulation of data contamination by tuning Qwen2.5-7B-Instruct on test samples from GSM8K and MATH, where ARC and MMLU can be regarded as OOD testing.

We observe that 1) the models show both higher MUI and performance on the contaminated datasets. 2) In specific, they first move in the coarsening direction — both performance and MUI decrease. As training steps increase, they gradually shift toward the accumulating direction and, on GSM8K, even show an evolving tendency. This trajectory mirrors the pattern induced by targeted capability optimization in the section 3.3. The resemblance is unsurprising: when leaked data come from the same domain, they effectively boost the model’s in-domain competence; with enough leaked samples, the effect becomes indistinguishable from specific ability enhancement. 3) By contrast, on OOD testing (i.e., ARC and MMLU), the models move along the collapsing direction. This reveals the key difference between data contamination and capability-specific optimization: overfitting to limited leaked samples raises MUI by encroaching on neurons responsible for OOD abilities, leading to simultaneous declines in both performance and MUI. That’s why we name this direction as collapsing. Therefore, data contamination and targeted capability optimization exhibit the same underlying dynamics; thus, Corollary 2 is not limited to contamination scenarios.

Takeaway: In summary, the ideal optimization trajectory during pre-training or post-training is the evolving direction. An accumulating trend signals insufficient training and warrants continued training; if it is accompanied by some coarsening, the data mix should be promptly rebalanced based on the fine-grained categories in the evaluation set. By contrast, the emergence of a collapsing direction calls for an immediate halt to training and a thorough inspection of the training and test sets for severe overfitting.

3.5 MUI for Model Comparison

Corollary 3. Model Comparison & Ranking: *On a fixed dataset, higher model performance is associated with lower model utilization, reflecting stronger foundational capabilities.*

In the previous sections, we present the common phenomenon revealed by the MUI–performance curve. In this section, we quantitatively demonstrate the effectiveness and stability of MUI from the aspect of model comparison. However, it is difficult to find out a universally accepted baseline for model ranking; for example, our observations show that even the Arena score is strongly biased toward response style and format, or highly correlated with mathematical reasoning tasks — exhibiting up to a 90% Pearson correlation with the GSM8K leaderboard regarding our selected models. Therefore, guided by Figure 3, we manually order nine base models: DeepSeek-Qwen2.5-7B, DeepSeek-Llama3.1-8B, Qwen2.5-7B-Instruct, Gemma-2-9B-Instruct, Llama-3.1-8B-Instruct, Llama-3-8B-Instruct, Qwen1.5-7B-Chat, Llama-2-7B-Chat, and Vicuna-7B as reference. Next, we design a simple composite metric that integrates MUI with performance and use it to reorder the same nine models. We then compute the correlation and variance between the two rankings: a higher correlation indicates a more reasonable ordering, while a smaller variance implies greater metric stability. Note that this composite metric is introduced solely for experimental convenience; devising a more principled aggregate metric is left to future work.

In specific, the combined metric is defined as the ratio of performance to MUI (PUR):

$$\text{PUR} = \frac{\mathcal{P}}{\text{MUI}^\alpha} \quad (7)$$

where α is a hyperparameter to punish MUI for balanced scale. We set it to 0.5 in experiments.

Model	GSM8K	MATH	ARC _c	HumanEval	MBPP	BBH	Ref./Avg	Correlation
Vicuna-7B	11.9 / 4.9	4.0 / 1.6	54.0 / 18.5	13.4 / 11.8	23.6 / 16.7	28.6 / 9.6		9
Llama-2-7B-Chat	25.8 / 12.4	5.4 / 2.3	60.0 / 23.9	16.4 / 16.4	24.8 / 19.0	26.2 / 8.9		8
Qwen1.5-7B-Chat	58.7 / 30.5	17.9 / 8.3	76.2 / 28.2	39.0 / 34.2	39.8 / 28.9	41.3 / 13.5		7
Llama-3-8B-Instruct	79.5 / 39.8	26.6 / 10.5	82.1 / 30.4	59.8 / 48.8	56.5 / 36.5	64.0 / 21.8		6
Llama-3.1-8B-Instruct	86.5 / 46.2	48.1 / 21.5	81.9 / 36.6	62.2 / 50.8	57.9 / 35.2	65.4 / 21.8		5
Gemma-2-9B-Instruct	82.3 / 51.0	33.5 / 16.2	89.5 / 41.3	63.4 / 66.8	61.2 / 50.0	57.5 / 23.3		4
Qwen2.5-7B-Instruct	84.5 / 55.7	61.9 / 33.1	86.8 / 37.4	71.3 / 75.2	62.1 / 49.1	66.0 / 25.7		3
DeepSeek-Llama3.1-8B	71.6 / 36.3	74.1 / 33.8	82.6 / 36.9	68.9 / 65.7	60.3 / 43.7	76.8 / 28.4		2
DeepSeek-Qwen2.5-7B	82.6 / 48.5	80.1 / 38.6	81.1 / 39.6	71.9 / 71.9	62.5 / 49.4	66.5 / 26.7		1
Spearman	68.3 / 75.0	98.3 / 98.3	66.7 / 88.3	98.3 / 91.7	95.0 / 86.7	91.7 / 96.2	86.4 _{Δ1.8}	89.4 _{Δ0.6}
Kendall	55.6 / 66.7	94.4 / 94.4	50.0 / 77.8	94.4 / 83.3	88.9 / 72.2	77.8 / 87.3	76.9 _{Δ3.2}	80.3 _{Δ0.9}

Table 1: Accuracy/PUR score (%) across six datasets. We exclude MMLU due to the inference cost. Ref is short for reference rank. All Spearman or Kendall coefficients are with < 0.02 p-value.

Table 1 shows the overall performance scores and the corresponding PUR values on six benchmark datasets. For evaluation, we establish two independent rankings of the nine LLMs. The first ranking is derived solely from raw performance and serves as the baseline that reflects conventional evaluation practice. The second ranking is obtained from the PUR scores, which jointly integrate MUI and performance. We then compute the correlation between each ranking and the manually curated reference. To quantify the agreement, we adopt Spearman’s correlation, which measures the strength of any monotonic relationship between two ranked lists, and Kendall’s coefficient, which evaluates the consistency of all pairwise orderings and is generally more robust to ties and outliers.

Our finds are as follows. 1) Higher correlation. The PUR-based ranking aligns more closely with the reference than the performance-based ranking, achieving average correlations of 89.4% versus 86.4% under Spearman, and 80.3% versus 76.9% under Kendall, thereby providing quantitative evidence of its effectiveness. 2) Lower variance. The PUR-based ranking exhibits smaller variance across datasets: 0.6 versus 1.8 (Spearman) and 0.9 versus 3.2 (Kendall), indicating that PUR delivers more stable ordering. 3) Qualitative improvements. Inspection of several ambiguous or previously mis-ranked cases (see Figure 3) shows how PUR resolves inconsistencies. For instance, although Vicuna and Llama-2 achieve nearly identical performance, MUI reveals Llama-2’s substantially greater underlying capability, allowing PUR to distinguish them; a similar clarification arises between Llama-3.1 and Qwen-2.5. Likewise, while Gemma-2 is generally regarded as stronger than Llama-3.1, a performance-only ranking suggests the opposite, whereas the PUR-based ranking corrects this by incorporating MUI.

3.6 MUI for Data Diversity Evaluation

Corollary 4. Positive Correlation Between Data Diversity and MUI: *As data diversity increases, encompassing various capabilities and domains, model utilization exhibits an upward trend.*

In the preceding sections we focused on the role of MUI in model evaluation; this section turns to data evaluation. Because MUI fundamentally measures the extent to which a test sample activates a model’s latent abilities, fixing the model allows us to invert the perspective: MUI can reveal which samples trigger different capabilities, serving as a model-specific indicator of data diversity.

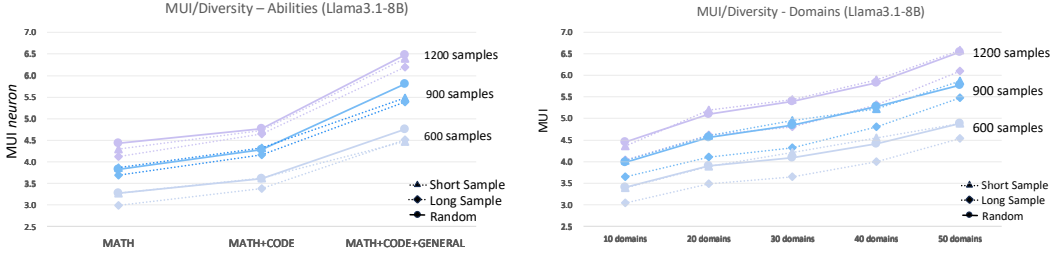


Figure 9: MUI across different data diversity dimensions: abilities and domains. Long or short samples are differentiated by 50% maximum length. The Mann-Whitney U test, at a 95% confidence level, the statistical significance analysis reveal that there are no statistically significant differences in proportions between short and long texts across the various dataset sizes.

There is no universally accepted definition of data diversity. Most existing work pursues diversity by balancing samples across capabilities or domains. We therefore experimentally examine the relationship between MUI and several conventional diversity dimensions. Note that a higher MUI indicates that a wider range of abilities has been activated, i.e., more diverse data. All experiments use Llama-3.1-7B-Instruct as the reference model and neuron-based MUI. Comparable findings for additional models, an analysis based on SAE interpretation, and experiments on more dimensions are provided in Appendix B.

For capability diversity, we following earlier experiments and consider three capabilities — mathematics, coding, and general abilities. From datasets covering different capability combinations, we randomly draw a fixed number of samples and compute their MUI, the results are shown in Figure 9. We can see that: 1) Overall, MUI shows a positive correlation with capability diversity. 2) Specifically, for similar capability combinations (from math to math+code), MUI grows slowly, whereas it rises rapidly when the combined capabilities are more dissimilar. 3) Roughly 600 samples spanning all three capabilities yield a MUI comparable to 1200 samples drawn from a single capability set, suggesting that MUI-guided sampling can substantially boost the efficiency of diversity selection. For domain diversity, we leverage existing labels from MMLU, BBH, MATH, and ARC. The results show similar trends. MUI is positively correlated with domain diversity. However, when we further stratify samples by length or difficulty (Appendix B.4), no significant trend emerges, implying that these factors are largely independent of the breadth of abilities a model can express.

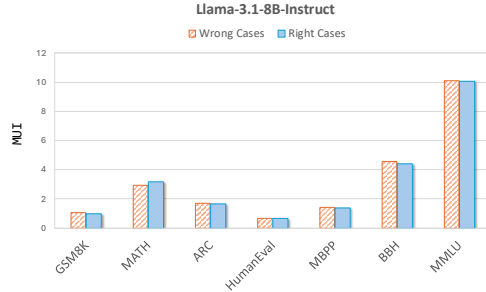


Figure 10: MUI for correct and incorrect responses for Llama-3.1-8B-Instruct.

3.7 Ablation on Response Correctness

We have utilized MUI to assess model capabilities and data diversity. However, there remains a significant issue to address to further validate the reliability of this metric — since MUI measures the activated capabilities, will it be affected by response quality, i.e., if only correct responses should

be considered as valid instances of capability utilization. We conduct an ablation study on MUI by sampling an equal number of correct and incorrect responses. The result using neuron-based MUI for Llama-3.1-8B-Instruct is shown in Figure 10, and additional results are provided in Appendix B.5. Using the Mann-Whitney U test, we find that there is no significant difference in MUI between correct and incorrect samples, demonstrating the reliability of MUI, no matter models can provide correct responses or not.

3.8 Impacts of Neuron Selection

MUI is designed to measure the fraction of task-activated features or neurons relative to the entire model, so the rule used to decide which neurons count as “activated” is crucial. Here we take neuron-based MUI as an example, SAE-based MUI adopts a similar strategy. As defined in Equation 3, we assign every neuron a contribution score that quantifies its influence on the output given the current input. Prior work [26, 12, 39] has employed three main thresholding strategies to identify key neurons: 1) Layer-level top-k (topk): selecting the k neurons with the highest contribution in each layer. 2) Global top-k (global_topk): selecting the top k neurons across the entire network. 3) Top-score (topscore): in each layer, selecting neurons whose contribution exceeds a fixed multiple of that layer’s maximum. More details are given in Appendix A.4.

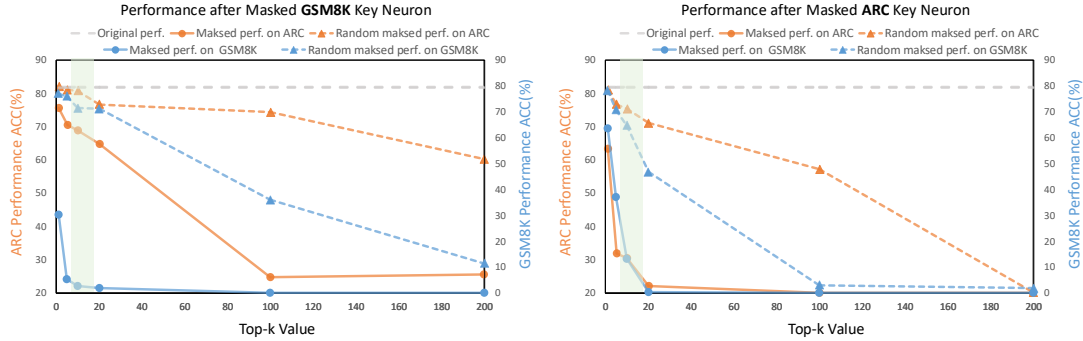


Figure 11: Performance of the Llama-3-8B-Instruct after the activated neurons being masked according to topk threshold. Left/right side selects activated neurons using ARC/GSM8K datasets. Our selection is based on the threshold marked in green box. Perf. is short for performance.

To keep MUI invariant to model size, we adopt a fixed ratio (i.e., the top one-thousandth) as the layer-level top-k threshold. Thus the numeric threshold varies across models and datasets. We validate this choice experimentally. Using Llama-3-8B-Instruct as base model and the ARC and GSM8K datasets, we progressively mask the neurons selected at different k values and present the resulting performance in Figures 11 (complete results appear in the Appendix B.6). Neuron masking is a widely used intervention technique in the field of mechanism interpretability that serves to verify whether a particular neuron bears a causal relationship to the model’s output. Ideally, the more task-relevant key neurons that are masked, the more pronounced the resulting performance degradation. We can see that 1) Masking neurons identified by either GSM8K or ARC causes performance to fall steadily as more neurons are removed, and the decline is far steeper than when an equal number of neurons is masked at random, confirming that the selected neurons are indeed task-critical. 2) Specifically, when neurons derived from ARC are masked, the performance curves on both datasets (blue for GSM8K and orange for ARC in the left figure) are almost identical: when $k \in (0, 20)$, they both decline rapidly. In contrast, when neurons derived from GSM8K are masked (right figure), only the GSM8K performance drops sharply, whereas the ARC performance decreases much more gradually. This is because ARC encompasses, but is not limited to, mathematical reasoning, which is the primary focus of GSM8K. Hence, our threshold evidently falls within this interval, enabling us to separate neurons associated with distinct capabilities.

3.9 Discussion

By leveraging the two mechanistic interpretability techniques (i.e., neuron-based and SAE-based) introduced above, we uncovered the Utility Law and its four corollaries, thereby demonstrating the

viability of using MUI for both model- and data-level evaluation. We also experimented with a variety of other neuron-probing methods to assess the generality of our approach. Results can be found in the Appendix B.6. However, interpretability remains a rapidly evolving field, and current technical constraints can make such extensions either difficult to implement or prone to metric instability. For example, when we switch to an SAE-based MUI, the scarcity of publicly available SAE models, the high cost of training new SAEs, and the need for layer-specific SAEs across different models restrict us to a very limited experimental set and preclude fair cross-model comparison. Likewise, replacing our present neuron-probing method still leaves the Model Utilization Law largely intact³, but a larger number of outliers emerge. These observations suggest that further investigation is needed on both fields.

4 Conclusion

We introduced MUI — a mechanism-interpretability metric that gauges how efficiently an LLM uses its capacity. Combined with performance, MUI offers an effective, stable, and generalizable analysis and evaluation for both model and data. Across various base models and benchmarks, we show a stable inverse, near-log MUI-performance curve, formalized as the Utility Law as well as four corollaries. Based on them, we discover four optimization directions during training — evolving, accumulating, coarsening, and collapsing — which clarify capability gains, specialization trade-offs, and data-contamination impacts. For model comparison, MUI produces model rankings that align closely with expert judgment while remaining variance-robust. For data diversity, we also show a positive correlation between MUI and various dimensions like domains and abilities, suggesting our metric as a model-specific comprehensive measurement. In the future, we are interested in engaging more advanced interpretability techniques for evaluation generalization, as well as leveraging MUI to guide model pre-training and post-training.

References

- [1] J. Austin, A. Odena, M. Nye, M. Bosma, H. Michalewski, D. Dohan, E. Jiang, C. Cai, M. Terry, Q. Le, et al. Program synthesis with large language models. *arXiv preprint arXiv:2108.07732*, 2021.
- [2] J. Bai, S. Bai, Y. Chu, and et. al. Qwen technical report. *arXiv preprint arXiv:2309.16609*, 2023.
- [3] B. bench authors. Beyond the imitation game: Quantifying and extrapolating the capabilities of language models. *Transactions on Machine Learning Research*, 2023. ISSN 2835-8856. URL <https://openreview.net/forum?id=uyTL5Bvosj>.
- [4] S. Bills, N. Cammarata, D. Mossing, H. Tillman, L. Gao, G. Goh, I. Sutskever, J. Leike, J. Wu, and W. Saunders. Language models can explain neurons in language models. <https://openaipublic.blob.core.windows.net/neuron-explainer/paper/index.html>, 2023.
- [5] T. Bricken, A. Templeton, J. Batson, B. Chen, A. Jermyn, T. Conerly, N. Turner, C. Anil, C. Denison, A. Askell, et al. Towards monosemanticity: Decomposing language models with dictionary learning. *Transformer Circuits Thread*, 2, 2023.
- [6] Y. Cao, S. Hong, X. Li, J. Ying, Y. Ma, H. Liang, Y. Liu, Z. Yao, X. Wang, D. Huang, et al. Toward generalizable evaluation in the llm era: A survey beyond benchmarks. *arXiv preprint arXiv:2504.18838*, 2025.
- [7] J. Chen, X. Wang, Z. Yao, Y. Bai, L. Hou, and J. Li. Finding safety neurons in large language models. *arXiv preprint arXiv:2406.14144*, 2024.
- [8] M. Chen, J. Tworek, H. Jun, and et. al. Evaluating large language models trained on code. *CoRR*, 2021.

³We obtain a preliminary average Pearson correlation coefficient of 0.78.

- [9] P. Clark, I. Cowhey, O. Etzioni, T. Khot, A. Sabharwal, C. Schoenick, and O. Tafjord. Think you have solved question answering? try arc, the ai2 reasoning challenge. *arXiv:1803.05457v1*, 2018.
- [10] K. Cobbe, V. Kosaraju, M. Bavarian, M. Chen, H. Jun, L. Kaiser, M. Plappert, J. Tworek, J. Hilton, R. Nakano, et al. Training verifiers to solve math word problems. *arXiv preprint arXiv:2110.14168*, 2021.
- [11] A. Conmy, A. Mavor-Parker, A. Lynch, S. Heimersheim, and A. Garriga-Alonso. Towards automated circuit discovery for mechanistic interpretability. *Advances in Neural Information Processing Systems*, 36:16318–16352, 2023.
- [12] D. Dai, L. Dong, Y. Hao, Z. Sui, B. Chang, and F. Wei. Knowledge neurons in pretrained transformers. In *Proceedings of the 60th Annual Meeting of the Association for Computational Linguistics (Volume 1: Long Papers)*, pages 8493–8502, 2022.
- [13] DeepSeek-AI. Deepseek-r1: Incentivizing reasoning capability in llms via reinforcement learning, 2025. URL <https://arxiv.org/abs/2501.12948>.
- [14] L. Gao, T. D. la Tour, H. Tillman, G. Goh, R. Troll, A. Radford, I. Sutskever, J. Leike, and J. Wu. Scaling and evaluating sparse autoencoders. *arXiv preprint arXiv:2406.04093*, 2024.
- [15] M. Geva, R. Schuster, J. Berant, and O. Levy. Transformer feed-forward layers are key-value memories. In *Proceedings of the 2021 Conference on Empirical Methods in Natural Language Processing*, pages 5484–5495, 2021.
- [16] M. Geva, A. Caciularu, K. Wang, and Y. Goldberg. Transformer feed-forward layers build predictions by promoting concepts in the vocabulary space. In *Proceedings of the 2022 Conference on Empirical Methods in Natural Language Processing*, pages 30–45, 2022.
- [17] A. Grattafiori, A. Dubey, A. Jauhri, and et. al. The llama 3 herd of models, 2024. URL <https://arxiv.org/abs/2407.21783>.
- [18] W. Gurnee, N. Nanda, M. Pauly, K. Harvey, D. Troitskii, and D. Bertsimas. Finding neurons in a haystack: Case studies with sparse probing. *Transactions on Machine Learning Research*, 2023.
- [19] Z. He, W. Shu, X. Ge, L. Chen, J. Wang, Y. Zhou, F. Liu, Q. Guo, X. Huang, Z. Wu, Y.-G. Jiang, and X. Qiu. Llama scope: Extracting millions of features from llama-3.1-8b with sparse autoencoders, 2024. URL <https://arxiv.org/abs/2410.20526>.
- [20] Z. He, W. Shu, X. Ge, L. Chen, J. Wang, Y. Zhou, F. Liu, Q. Guo, X. Huang, Z. Wu, et al. Llama scope: Extracting millions of features from llama-3.1-8b with sparse autoencoders. *arXiv preprint arXiv:2410.20526*, 2024.
- [21] D. Hendrycks, C. Burns, S. Basart, A. Zou, M. Mazeika, D. Song, and J. Steinhardt. Measuring massive multitask language understanding. *arXiv preprint arXiv:2009.03300*, 2020.
- [22] D. Hendrycks, C. Burns, S. Kadavath, A. Arora, S. Basart, E. Tang, D. Song, and J. Steinhardt. Measuring mathematical problem solving with the math dataset. *NeurIPS*, 2021.
- [23] B. Hui, J. Yang, Z. Cui, J. Yang, D. Liu, L. Zhang, T. Liu, J. Zhang, B. Yu, K. Dang, et al. Qwen2. 5-coder technical report. *arXiv preprint arXiv:2409.12186*, 2024.
- [24] T. Lieberum, S. Rajamanoharan, A. Conmy, L. Smith, N. Sonnerat, V. Varma, J. Kramár, A. Dragan, R. Shah, and N. Nanda. Gemma scope: Open sparse autoencoders everywhere all at once on gemma 2. *arXiv preprint arXiv:2408.05147*, 2024.
- [25] T. Lieberum, S. Rajamanoharan, A. Conmy, L. Smith, N. Sonnerat, V. Varma, J. Kramar, A. Dragan, R. Shah, and N. Nanda. Gemma scope: Open sparse autoencoders everywhere all at once on gemma 2. In Y. Belinkov, N. Kim, J. Jumelet, H. Mohebbi, A. Mueller, and H. Chen, editors, *Proceedings of the 7th BlackboxNLP Workshop: Analyzing and Interpreting Neural Networks for NLP*, pages 278–300, Miami, Florida, US, Nov. 2024. Association for Computational Linguistics. doi: 10.18653/v1/2024.blackboxnlp-1.19. URL <https://aclanthology.org/2024.blackboxnlp-1.19/>.

- [26] K. Meng, D. Bau, A. Andonian, and Y. Belinkov. Locating and editing factual associations in gpt. *Advances in Neural Information Processing Systems*, 35:17359–17372, 2022.
- [27] T. OLMO, P. Walsh, L. Soldaini, D. Groeneveld, K. Lo, S. Arora, A. Bhagia, Y. Gu, S. Huang, M. Jordan, N. Lambert, D. Schwenk, O. Tafjord, T. Anderson, D. Atkinson, F. Brahman, C. Clark, P. Dasigi, N. Dziri, M. Guerquin, H. Ivison, P. W. Koh, J. Liu, S. Malik, W. Merrill, L. J. V. Miranda, J. Morrison, T. Murray, C. Nam, V. Pyatkin, A. Rangapur, M. Schmitz, S. Skjonsberg, D. Wadden, C. Wilhelm, M. Wilson, L. Zettlemoyer, A. Farhadi, N. A. Smith, and H. Hajishirzi. 2 olmo 2 furious, 2024. URL <https://arxiv.org/abs/2501.00656>.
- [28] H. Pan, Y. Cao, X. Wang, and X. Yang. Finding and editing multi-modal neurons in pre-trained transformer. *arXiv preprint arXiv:2311.07470*, 2023.
- [29] B. Peng, C. Li, P. He, M. Galley, and J. Gao. Instruction tuning with gpt-4, 2023. URL <https://arxiv.org/abs/2304.03277>.
- [30] B. Rozière, J. Gehring, F. Gloeckle, S. Sootla, I. Gat, X. E. Tan, Y. Adi, J. Liu, R. Sauvestre, T. Remez, J. Rapin, A. Kozhevnikov, I. Evtimov, J. Bitton, M. Bhatt, C. C. Ferrer, A. Grattafiori, W. Xiong, A. Défossez, J. Copet, F. Azhar, H. Touvron, L. Martin, N. Usunier, T. Scialom, and G. Synnaeve. Code llama: Open foundation models for code, 2024. URL <https://arxiv.org/abs/2308.12950>.
- [31] G. Team. Gemma 2: Improving open language models at a practical size, 2024. URL <https://arxiv.org/abs/2408.00118>.
- [32] Q. Team. Qwen2.5: A party of foundation models, September 2024. URL <https://qwenlm.github.io/blog/qwen2.5/>.
- [33] H. Touvron, L. Martin, K. Stone, and et. al. Llama 2: Open foundation and fine-tuned chat models, 2023. URL <https://arxiv.org/abs/2307.09288>.
- [34] J. Vig, S. Gehrmann, Y. Belinkov, S. Qian, D. Nevo, Y. Singer, and S. Shieber. Investigating gender bias in language models using causal mediation analysis. *Advances in neural information processing systems*, 33:12388–12401, 2020.
- [35] X. Wang, K. Wen, Z. Zhang, L. Hou, Z. Liu, and J. Li. Finding skill neurons in pre-trained transformer-based language models. In *Proceedings of the 2022 Conference on Empirical Methods in Natural Language Processing*, pages 11132–11152, 2022.
- [36] A. Yang, B. Zhang, B. Hui, B. Gao, B. Yu, C. Li, D. Liu, J. Tu, J. Zhou, J. Lin, K. Lu, M. Xue, R. Lin, T. Liu, X. Ren, and Z. Zhang. Qwen2.5-math technical report: Toward mathematical expert model via self-improvement. *arXiv preprint arXiv:2409.12122*, 2024.
- [37] J. Ying, Y. Cao, Y. Bai, Q. Sun, B. Wang, W. Tang, Z. Ding, Y. Yang, X. Huang, and S. Yan. Automating dataset updates towards reliable and timely evaluation of large language models. In A. Globerson, L. Mackey, D. Belgrave, A. Fan, U. Paquet, J. Tomczak, and C. Zhang, editors, *Advances in Neural Information Processing Systems*, volume 37, pages 17106–17132. Curran Associates, Inc., 2024. URL https://proceedings.neurips.cc/paper_files/paper/2024/file/1e89c12621c0315373f20f0aeabe5dbe-Paper-Datasets_and_Benchmarks_Track.pdf.
- [38] J. Ying, M. Lin, Y. Cao, W. Tang, B. Wang, Q. Sun, X. Huang, and S. Yan. LLMs-as-instructors: Learning from errors toward automating model improvement. In Y. Al-Onaizan, M. Bansal, and Y.-N. Chen, editors, *Findings of the Association for Computational Linguistics: EMNLP 2024*, pages 11185–11208, Miami, Florida, USA, Nov. 2024. Association for Computational Linguistics. doi: 10.18653/v1/2024.findings-emnlp.654. URL <https://aclanthology.org/2024.findings-emnlp.654/>.
- [39] Y. Zhao, W. Zhang, G. Chen, K. Kawaguchi, and L. Bing. How do large language models handle multilingualism? *arXiv preprint arXiv:2402.18815*, 2024.

A Experiment Details

A.1 Dataset Statistical Result

Following [17], we focus on three key abilities: Mathematical and Reasoning, Coding, and General Capability. For each ability, we select several publicly available datasets to explore the Utility Law. Table 2 provides a detailed summary of the statistical characteristics of the selected datasets.

Model	GSM8K (Math & Reasoning)	MATH (Math & Reasoning)	ARC _c (Math & Reasoning)	HumanEval (Code)	MBPP (Code)	BBH (General)	MMLU (General)	Totally
# Testing Samples	1,319	5,000	1,172	164	500	6,511	14,042	28,708

Table 2: The statistical detail of the selected benchmarks.

A.2 OLMo Series Model Selection

For OLMo [27] series model, we include eight checkpoints detailed in Table 3.

Custom Checkpoint Name	Original Checkpoint Name	Training Steps	Training Tokens	Traning Stage
OLMo-2-7B-0.5T	stage1-step122000-tokens512B	122,000	512B	1
OLMo-2-7B-1T	stage1-step244000-tokens1024B	244,000	1,024B	1
OLMo-2-7B-1.5T	stage1-step366000-tokens1536B	366,000	1,536B	1
OLMo-2-7B-2T	stage1-step488000-tokens2047B	488,000	2,047B	1
OLMo-2-7B-2.5T	stage1-step610000-tokens2559B	610,000	2,559B	1
OLMo-2-7B-3T	stage1-step732000-tokens3071B	732,000	3,071B	1
OLMo-2-7B-3.5T	stage1-step855000-tokens3587B	855,000	3,587B	1
OLMo-2-7B-4T	OLMo-2-1124-7B	928,646	3,896B	1

Table 3: Summary of the checkpoints of model OLMo-2-1124-7B used in the study. “Custom Checkpoint Name” represents simplified names defined in this paper for clarity.

A.3 Mechanistic Interpretability Techniques

For neuron analysis, we primarily follow one of the most commonly used methods, as described in Section 2.1.1, due to time and cost considerations. However, we emphasize that our approach is not limited to a fixed neuron analysis method. Instead, we aim to explore MUI using multiple techniques, to ensure a comprehensive and robust analysis. In our ablation study in Section B.6.3, we deploy other neuron analysis methods to further investigate and validate our findings. When using the method defined in Section 2.1.1, the response y_i in Equation 3, are generated under specific conditions depending on the benchmark. For BBH, 3-shot examples from the original benchmark are used. For all other benchmarks, responses are generated in a zero-shot manner for instruction-tuned models, while a human-crafted one-shot setting is used for all the base models. Details of the model generate configuration and the few-shot examples are provided in Appendix A.6. The η in Equation 3, is set to the top 1% of key neurons and selected at the layer level (corresponding to the top 1% of N). This threshold function is detailed as follows:

$$N_{\text{neuron}}(t) = \left\{ (i, l) \mid f_{\text{neuron}}(i, l, \hat{y}_j \mid x + \hat{y}_{<j}) \geq V_l^{\text{top}1\%}, \hat{y}_j \in y, l \in \{1, 2, \dots, L\}, i \in \{1, 2, \dots, N\} \right\}, \quad (8)$$

where $V_l = [f_{\text{neuron}}(i, l, \hat{y}_j \mid x + \hat{y}_{<j}) \mid \hat{y}_j \in y, i \in \{1, 2, \dots, N\}]$, with L representing the number of layers and N the number of neurons in the tested model.

Regarding using SAE to conduct analysis: we utilized all publicly available LLMs with SAEs for our analysis, including Llama3.1-8B with Llama Scope SAE [19] and Gemma-2-9B & Gemma-2-9B-Instruct with SAE from Gemma Scope [25]. The response generation process for y_i in Equation 6 follows the same procedure as described in the neuron analysis technique. To ensure a convenient and as fair as possible comparison of model utilization across different architectures, we selected the Residual SAE with the width of 128K for each possible layer. Considering that the SAEs trained by Llama Scope use the Top50-ReLU activation function, while those from Gemma Scope adopt JumpReLU, we adjusted the selection criteria for the Gemma SAEs. Specifically, for each layer in Gemma, we selected SAEs with an L_0 close to 50 to align with the Llama Scope configuration.

Detailed parameter selection is shown in Appendix A.5. The η in Equation 6, is set to the top 50 of features and selected at the layer level. This threshold function is detailed as follows:

$$N_{\text{sac}}(t) = \left\{ (i, l) \mid f_{\text{sac}}(i, l, \hat{y}_j \mid x + \hat{y}_{<j}) \geq V_l^{\text{top}50}, \hat{y}_j \in y, l \in \{1, 2, \dots, L\}, i \in \{1, 2, \dots, D\} \right\}, \quad (9)$$

where $V_l = [f_{\text{sac}}(i, l, \hat{y}_j \mid x_i + \hat{y}_{<j}) \mid \hat{y}_j \in y, i \in \{1, 2, \dots, D\}]$, with L representing the number of layers and D the number of features in Equation 4.

A.4 Implementation for Threshold Function

Generally, there are several different threshold functions implemented for η , two of which have been introduced in Appendix A.3. Here, we uniformly represent these methods within the context of neuron and SAE interpretation:

- **Top-k:** that we select neurons that have the top k values for each layer, as defined by:

$$N_{\text{neuron/sac}}(t) = \left\{ (i, l) \mid f_{\text{neuron/sac}}(i, l, \hat{y}_j \mid x + \hat{y}_{<j}) \geq V_l^{\text{top}k}, \hat{y}_j \in y, l \in \{1, 2, \dots, L\}, i \in \{1, 2, \dots, N/D\} \right\}, \quad (10)$$

where, $V_l = [f_{\text{neuron/sac}}(i, l, \hat{y}_j \mid x_i + \hat{y}_{<j}) \mid \hat{y}_j \in y, i \in \{1, 2, \dots, N/D\}]$

- **Global Top-k:** is a similar approach but selecting top values across all layers:

$$N_{\text{neuron/sac}}(t) = \left\{ (i, l) \mid f_{\text{neuron/sac}}(i, l, \hat{y}_j \mid x + \hat{y}_{<j}) \geq V^{\text{top}k}, \hat{y}_j \in y, l \in \{1, 2, \dots, L\}, i \in \{1, 2, \dots, N/D\} \right\}, \quad (11)$$

where $V = [f_{\text{neuron/sac}}(i, l, \hat{y}_j \mid x_i + \hat{y}_{<j}) \mid \hat{y}_j \in y, l \in \{1, 2, \dots, L\}, i \in \{1, 2, \dots, N/D\}]$

- **Top-%k:** similar to the top-k method, this approach uses a fixed percentage, $k\%$, multiplied by N/D to determine the threshold. This modification can alleviate discrepancies due to different model architectures when calculating the MUI. Specifically, when calculating the MUI, if the denominator N_{total} is defined as $N_{\text{total}} = N/D \times L$, setting the threshold as a proportion of N/D helps mitigate issues caused by varying model structures. This ensures a more equitable comparison across various models.

- **Top-score:** as Dai et al. [12], using a fraction k of the maximum attribution score for each layer:

$$N_{\text{neuron/sac}}(t) = \left\{ (i, l) \mid f_{\text{neuron/sac}}(i, l, \hat{y}_j \mid x + \hat{y}_{<j}) \geq kV_l^{\text{max}}, \hat{y}_j \in y, l \in \{1, 2, \dots, L\}, i \in \{1, 2, \dots, N/D\} \right\}, \quad (12)$$

where V_l^{max} is the maximum value in V_l .

Here to notice, V_l and V are token-level calculation, if using a sponse-level score (Equation 15) the V_l will be as $V_l = [f_{\text{neuron/sac_sum}}(i, l, y \mid x) \mid i \in \{1, 2, \dots, N/D\}]$ correspondingly.

A.5 Sparse-Autoencoder (SAE) Selection

Table A.5 shows the detailed parameter information of the selected SAEs.

Models	Llama-3.1-8B-Base	Gemma-2-9B-Base
Trained BY	Llama Scope	Gemma Scope
SAE Position (Layer)	Every Layer	Every Layer
SAE Position (Site)	Residual	Residual
SAE Width (# Features)	128K	128K
Activation Function	TopK-ReLU	JumpReLU

Table 4: An overview of selected SAEs on Large Language Models.

A.6 Model Parameter Setting

- **Response Generation:** across all involved models is conducted with a fixed temperature of 0.0 (*do_sample=False*) and a maximum token length of 1024 (8192 for DeepSeek-Llama3.1-8B and DeepSeek-Qwen2.5-7B). The generation conditions vary depending on the benchmark. For BBH, 3-shot examples from the original benchmark are used. For all other benchmarks, responses are generated in a zero-shot manner for instruction-tuned models, while a human-crafted one-shot setting is applied for base models. The human-crafted few-shot example is shown in Appendix C.
- **SAE Analysis:** To ensure consistency and fairness in our evaluations, we truncate inputs to a maximum token length of 2048, as dictated by Llama Scope’s encoder limitations. Consequently, tasks with few-shot examples from the BBH dataset, which require substantial response truncation, are excluded from our analysis.
- **Full Parameter Fine-tuning:** Following work [37], we train the model on selected code-related tasks (HumanEval and MBPP) and math-related tasks (GSM8K and MATH). During full parameter fine-tuning (STF), test samples are concatenated with answers. This fine-tuning process involves adjusting several parameters: the learning rate, which varies from 7×10^{-5} to 2×10^{-9} ; the number of epochs, ranging from 2 to 4; and the batch size, set between 4 and 128. The optimal performance for each model configuration are identified. The experiment is conducted on 8 NVIDIA H20 GPUs.

B More Experiment Results

B.1 Utility Law: the Relationship Between MUI and Performance

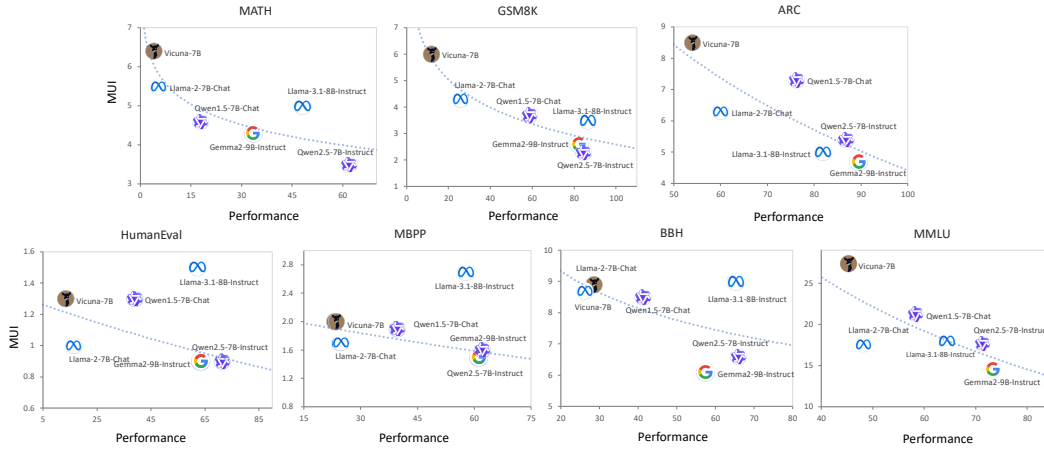


Figure 12: Performance (accuracy %) and Model Utilization Index (MUI) (%), as determined by neuron analysis (refer to Section 2.1.1), of the selected six models across the selected seven tasks. Results indicate that models with stronger performance activate fewer features for the corresponding tasks. The dashed line represents the trend line fitted using a logarithmic function.

Model	GSM8K (Math & Reasoning)	MATH (Math & Reasoning)	ARC _c (Math & Reasoning)	HumanEval (Code)	MBPP (Code)	BBH (General)	MMLU (General)
Vicuna-7B	11.9 / 6.0	4.0 / 6.4	54.0 / 8.5	13.4 / 1.3	23.6 / 2.0	28.6 / 8.9	45.3 / 27.4
Llama-2-7B-Chat	25.8 / 4.3	5.4 / 5.5	60.0 / 6.3	16.4 / 1.0	24.8 / 1.7	26.2 / 8.7	48.2 / 17.6
CodeLlama-7B-Instruct	23.0 / 5.1	6.0 / 8.0	49.5 / 9.6	34.1 / 2.0	44.7 / 3.3	21.8 / 8.5	41.4 / 26.3
Qwen1.5-7B-Chat	58.7 / 3.7	17.9 / 4.6	76.2 / 7.3	39.0 / 1.3	39.8 / 1.9	41.3 / 9.4	58.3 / 21.3
Llama-3.1-8B-Instruct	86.5 / 3.5	48.1 / 5.0	81.9 / 5.0	62.2 / 1.5	57.9 / 2.7	65.4 / 9.0	64.4 / 18.0
Gemma2-9B-Instruct	82.3 / 2.6	33.5 / 4.3	89.5 / 4.7	63.4 / 0.9	61.2 / 1.5	57.5 / 6.1	73.3 / 14.6
Qwen2.5-7B-Instruct	84.5 / 2.3	61.9 / 3.5	86.8 / 5.4	71.3 / 0.9	62.1 / 1.6	66.0 / 6.6	71.3 / 17.7
Qwen2.5-Coder-7B-Instruct	79.6 / 4.3	49.5 / 7.5	83.8 / 11.1	75.0 / 1.8	65.9 / 3.0	57.8 / 13.1	65.6 / 34.4
Qwen2.5-Math-7B-Instruct	92.1 / 2.3	76.7 / 4.0	66.3 / 3.3	53.0 / 1.0	47.9 / 1.5	29.1 / 3.7	51.2 / 17.3
DeepSeek-Llama3.1-8B	71.6 / 3.9	74.1 / 4.8	82.6 / 5.0	68.9 / 1.1	60.3 / 1.9	76.8 / 7.3	-
DeepSeek-Qwen2.5-7B	82.6 / 2.9	80.1 / 4.3	81.1 / 4.2	71.9 / 1.0	62.5 / 1.6	66.5 / 6.2	-
Vicuna-13B	22.4 / 4.6	5.0 / 5.5	61.9 / 8.3	17.1 / 1.3	27.6 / 2.0	42.3 / 7.0	50.9 / 26.7
Llama-2-13B-Chat	36.2 / 4.1	7.4 / 4.9	66.8 / 6.0	18.9 / 1.1	29.7 / 1.6	26.1 / 8.2	53.6 / 16.5
Qwen1.5-14B-Chat	70.7 / 5.4	25.6 / 7.4	86.3 / 10.1	50.6 / 1.7	49.9 / 2.7	50.3 / 13.4	65.4 / 32.7
Qwen2.5-14B-Instruct	84.7 / 5.3	60.9 / 7.7	91.5 / 10.0	68.3 / 1.9	63.3 / 3.3	64.0 / 13.2	77.2 / 31.1
Qwen2.5-Coder-14B-Instruct	86.3 / 4.5	55.7 / 7.4	88.4 / 10.2	81.1 / 1.8	67.3 / 3.1	71.7 / 12.5	71.0 / 31.5

Table 5: Performance (accuracy %) and Model Utilization Index (MUI) (%), as determined by neuron analysis. More detailed experiment settings can be found in Appendix A.3.

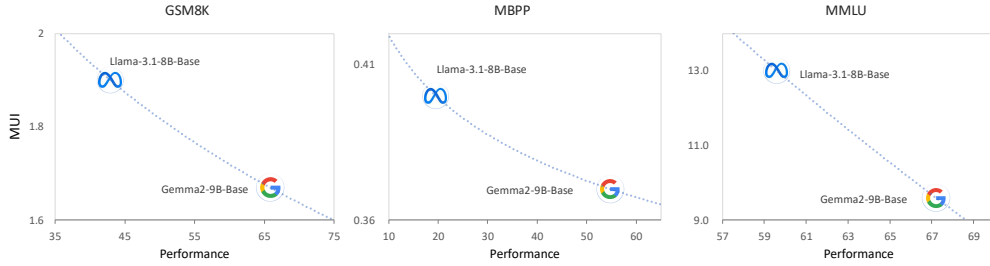


Figure 13: Relationship between performance (accuracy) and SAE-based MUI. The dashed line represents the trend line fitted using a logarithmic function. More results can be found in Table 6.

Model	GSM8K (Math & Reasoning)	MATH (Math & Reasoning)	ARC _c (Math & Reasoning)	HumanEval (Code)	MBPP (Code)	BBH (General)	MMLU (General)
Llama-3.1-8B	42.9 / 1.9	15.1 / 2.0	77.1 / 3.2	19.5 / 0.40	26.1 / 0.7	50.1 / 3.9	59.6 / 13.0
Gemma2-9B	65.8 / 1.7	20.8 / 2.4	84.6 / 3.2	54.8 / 0.37	57.7 / 0.5	67.4 / 2.2	67.2 / 9.6

Table 6: Performance (accuracy %) under one-shot inference setting / SAE-based Model Utilization Index (MUI) (%) of the selected model. Detailed experiment settings can be found in Appendix A.3.

Model	GSM8K (Math & Reasoning)	MATH (Math & Reasoning)	ARC _c (Math & Reasoning)	HumanEval (Code)	MBPP (Code)	BBH (General)	MMLU (General)
Gemma2-9B	4.2180	3.8527	4.6095	3.6149	3.5155	3.9860	4.7394
Llama-3.1-8B	0.034	0.031	0.034	0.029	0.0295	0.0302	0.0356

Table 7: Reconstruction Loss when conducting experiments for SAE-Based Model Utilization Index (MUI) analysis using Llama and Gemma Models

B.2 Corollary 1. Regression Testing Metrics for Model Training

Model	GSM8K (Math & Reasoning)	MATH (Math & Reasoning)	ARC _c (Math & Reasoning)	HumanEval (Code)	MBPP (Code)	BBH (General)	MMLU (General)
OLMo-2-7B-0.5T	7.6 / 6.4	3.8 / 5.5	52.3 / 7.4	4.3 / 0.8	8.2 / 1.1	23.3 / 6.0	42.5 / 16.7
OLMo-2-7B-1T	8.0 / 4.3	4.2 / 6.5	59.6 / 8.2	4.8 / 1.0	10.6 / 1.5	27.1 / 7.2	45.2 / 20.7
OLMo-2-7B-1.5T	10.8 / 6.3	4.7 / 8.6	62.2 / 9.4	9.7 / 1.1	14.8 / 1.8	27.3 / 8.5	49.1 / 24.1
OLMo-2-7B-2T	13.5 / 4.8	4.8 / 7.3	66.0 / 9.4	9.1 / 1.2	15.0 / 1.9	30.9 / 8.3	50.7 / 23.9
OLMo-2-7B-2.5T	15.2 / 6.8	5.5 / 7.3	66.0 / 9.8	6.7 / 1.2	15.8 / 2.0	35.0 / 8.9	51.2 / 24.3
OLMo-2-7B-3T	15.3 / 6.1	5.3 / 7.6	71.2 / 9.6	9.1 / 1.3	18.8 / 2.0	35.1 / 8.8	53.2 / 25.6
OLMo-2-7B-3.5T	16.8 / 5.4	5.7 / 6.5	71.4 / 9.1	8.5 / 1.2	20.8 / 1.9	38.5 / 8.0	53.7 / 23.8
OLMo-2-7B-4T (final)	68.2 / 5.1	15.4 / 6.5	79.8 / 9.4	19.5 / 1.2	29.3 / 1.8	46.5 / 8.2	59.2 / 24.0

Table 8: Performance (accuracy %) under few-shot inference setting / Model Utilization Index (MUI) (%) of the OLMo series model. The detailed checkpoint information is shown in Appendix A.2.

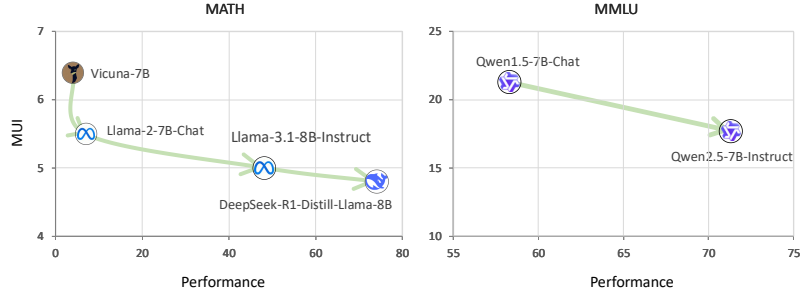


Figure 14: MUI (%) and Performance ACC (%) change trend compared between model Vicuna-7B, Llama-2-7B-Chat, Llama-3.1-8B-Instruct, and DeepSeek-R1-Distill-Llama-8, as well as between Qwen1.5-7B-Chat and Qwen2.5-7B-Instruct on task MATH and MMLU. The continual improvements in capabilities is reflected by a consistent decrease in MUI and an increase in performance.

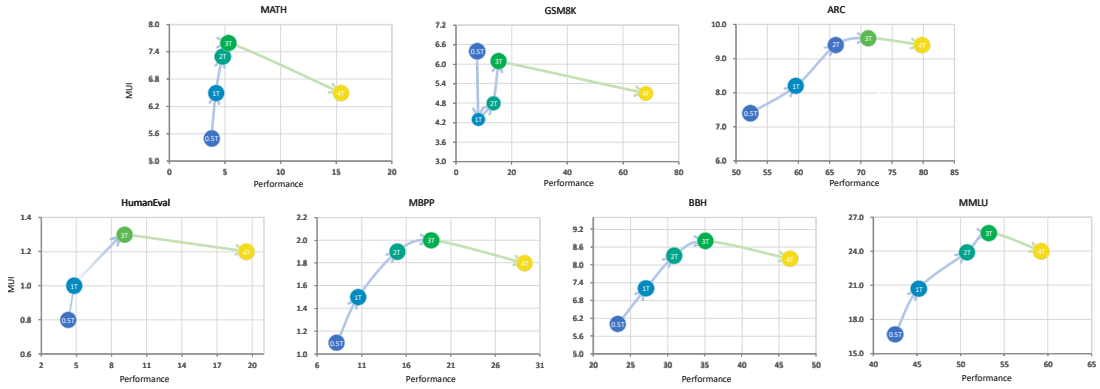


Figure 15: Performance (accuracy %) and Model Utilization Index (MUI) (%) of the OLMo series model across the Selected Seven Tasks.

Model	GSM8K (Math & Reasoning)	MATH (Math & Reasoning)	ARC _c (Math & Reasoning)	HumanEval (Code)	MBPP (Code)	BBH (General)	MMLU (General)
Llama-2-7B-Chat	25.8 / 4.3	5.4 / 5.5	60.0 / 6.3	16.4 / 1.0	24.8 / 1.7	26.2 / 8.7	48.2 / 17.6
CodeLlama-7B-Instruct	23.0 / 5.1	6.0 / 8.0	49.5 / 9.6	34.1 / 2.0	44.7 / 3.3	21.8 / 8.5	41.4 / 26.3
Qwen2.5-7B-Instruct	84.5 / 2.3	61.9 / 3.5	86.8 / 5.4	71.3 / 0.9	62.1 / 1.6	66.0 / 6.6	71.3 / 17.7
Qwen2.5-Coder-7B-Instruct	79.6 / 4.3	49.5 / 7.5	83.8 / 11.1	75.0 / 1.8	65.9 / 3.0	57.8 / 13.1	65.6 / 34.4
Qwen2.5-Math-7B-Instruct	92.1 / 2.3	76.7 / 4.0	66.3 / 3.3	53.0 / 1.0	47.9 / 1.5	29.1 / 3.7	51.2 / 17.3

Table 9: Performance (accuracy %) and Model Utilization Index (MUI) (%), as determined by neuron analysis for Llama-2-7B-Chat, CodeLlama-7B-Instruct, Qwen2.5-7B-Instruct, Qwen2.5-Coder-7B-Instruct, and Qwen2.5-Math-7B-Instruct.

B.3 Corollary 2. Data Contamination Detection

Model	GSM8K (Math & Reasoning)	MATH (Math & Reasoning)	ARC _c (Math & Reasoning)	HumanEval (Code)	MBPP (Code)	BBH (General)	MLLU (General)
Llama-2-7B-Chat	25.8 / 4.3	5.4 / 5.5	60.0 / 6.3	16.4 / 1.0	24.8 / 1.7	26.2 / 8.7	48.2 / 17.6
Llama-Code-Leakage	22.2 / 4.3	5.2 / 4.8	60.7 / 5.2	35.4 / 2.2	49.7 / 1.5	23.6 / 7.7	48.1 / 15.6
Llama-Math-Leakage	39.0 / 4.6	8.2 / 6.4	49.5 / 8.2	5.5 / 1.0	8.6 / 2.0	25.2 / 6.6	43.9 / 25.8
Llama-3.1-8B-Instruct	86.5 / 3.5	48.1 / 5.0	81.9 / 5.0	62.2 / 1.5	57.9 / 2.7	65.4 / 9.0	64.4 / 18.0
Llama3.1-Code-Leakage	86.6 / 4.0	40.2 / 5.5	81.2 / 6.2	81.7 / 1.6	69.1 / 2.4	48.1 / 8.2	66.3 / 18.5
Llama3.1-Math-Leakage	89.8 / 3.8	47.4 / 5.2	81.6 / 5.9	54.9 / 1.8	50.5 / 2.5	48.9 / 7.6	66.1 / 18.0
Qwen2.5-7B-Instruct	84.5 / 2.4	61.9 / 3.5	86.8 / 5.4	71.3 / 0.9	62.1 / 1.6	66.0 / 6.6	71.3 / 17.7
Qwen2.5-Code-Leakage	78.6 / 2.0	42.5 / 3.7	88.9 / 5.6	85.4 / 1.9	73.5 / 2.0	56.8 / 6.7	56.8 / 14.5
Qwen2.5-Math-Leakage	98.1 / 2.8	84.6 / 4.1	57.4 / 4.5	2.2 / 1.0	1.8 / 1.7	31.4 / 6.1	44.7 / 14.2

Table 10: Performance (accuracy %) and Model Utilization Index (MUI) (%) for Llama-2-7B-Chat, Llama-3.1-8B-Instruct, and Qwen2.5-7B-Instruct, including their post-data contamination training performance on code-related tasks (HumanEval and MBPP) and math-related tasks (MATH and GSM8K). The detailed training setting is shown in Appendix A.6.

B.4 Corollary 4. Positive Correlation Between Data Diversity and MUI

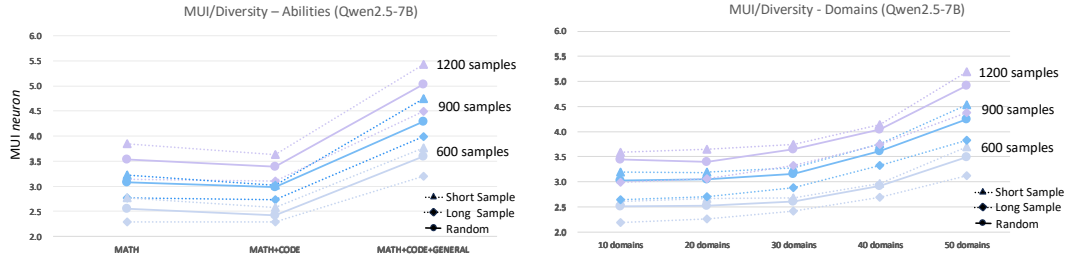


Figure 16: Using the Mann-Whitney U test, we evaluate the statistical significance of differences in MUI across different dataset sizes (600, 900, 1200) and text lengths (short vs. long) when using evaluation data testing different abilities. At a 95% confidence level, the analysis reveals that there are no statistically significant differences in proportions between short and long texts across the various dataset sizes. All p-values exceed the 0.05 threshold, indicating that text length does not significantly impact the MUI under these conditions.

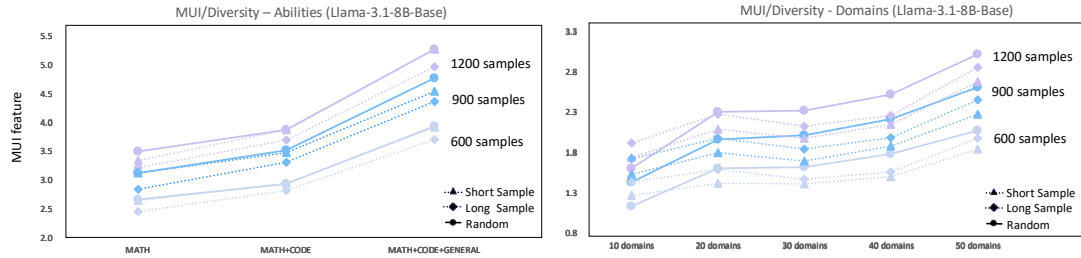


Figure 17: Using the Mann-Whitney U test, we evaluate the statistical significance of differences in MUI across different dataset sizes (600, 900, 1200) and text lengths (short vs. long) when using evaluation data testing different abilities. At a 95% confidence level, the analysis reveals that there are no statistically significant differences in proportions between short and long texts across the various dataset sizes. All p-values exceed the 0.05 threshold, indicating that text length does not significantly impact the MUI under these conditions.

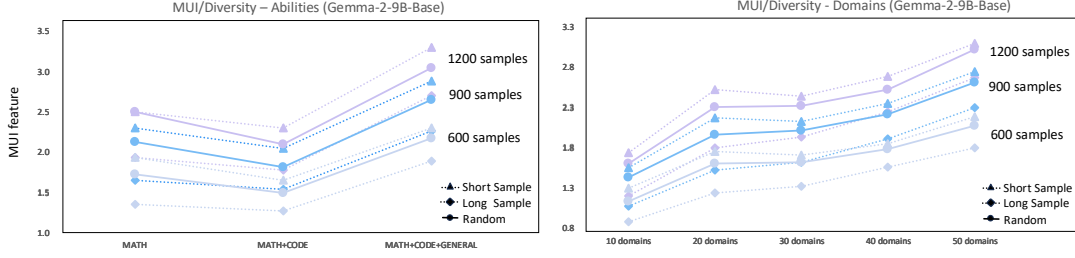


Figure 18: Using the Mann-Whitney U test, we evaluate the statistical significance of differences in MUI across different dataset sizes (600, 900, 1200) and text lengths (short vs. long) when using evaluation data testing different abilities. At a 95% confidence level, the analysis reveals that there are no statistically significant differences in proportions between short and long texts across the various dataset sizes. All p-values exceed the 0.05 threshold, indicating that text length does not significantly impact the MUI under these conditions.

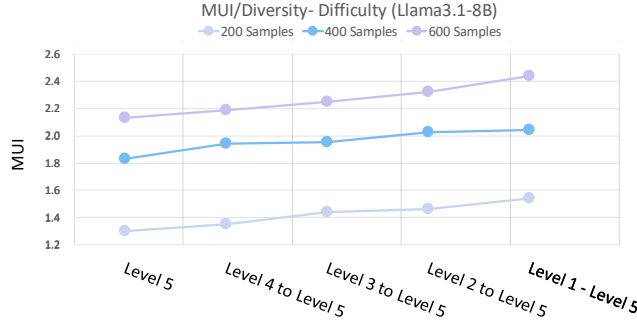


Figure 19: MUI (%) across various dataset sizes (200, 400, 600) and question difficulty levels evaluated on the MATH dataset. “Level x to Level y” denotes a uniform distribution of questions ranging from difficulty level x to y. The results suggest that merely increasing the difficulty does not enhance the MUI — the MUI for the highest difficulty level (level 5) is lower than the MUI across questions equally from levels 1 through 5.

B.5 Ablation on Answer Correctness

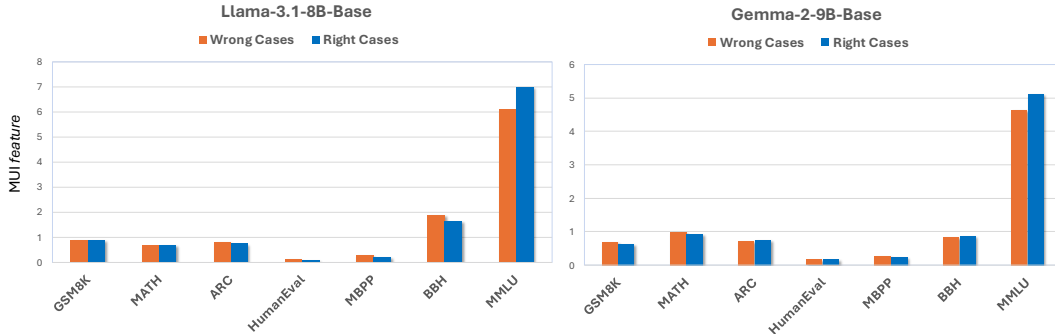


Figure 20: Ablation Study: the $MUI_{feature}$ for model Llama-3.1-8B-Base and Gemma-2-9B-Base, evaluated on correct and incorrect cases from the seven tasks. The Mann-Whitney U test indicates no significant differences between MUI on correct and incorrect cases for the two models.

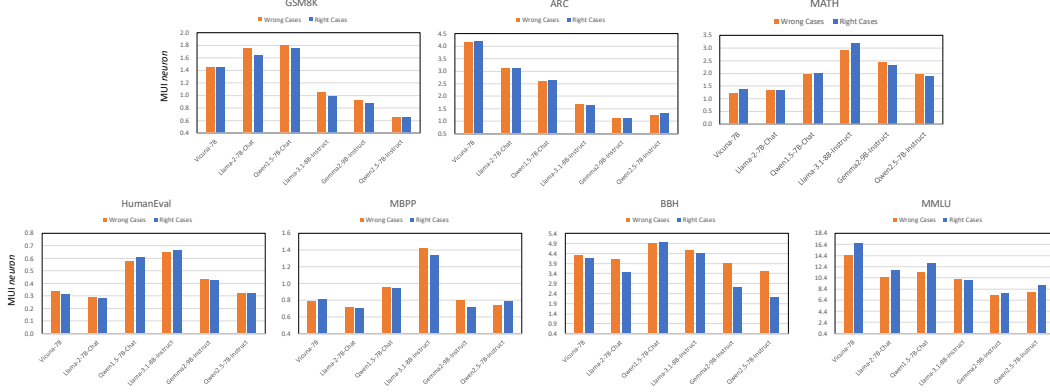


Figure 21: Ablation Study: the MUI_{neuron} for seven model evaluated on correct and incorrect cases from the seven tasks (more detailed experiment setting is shown in Section 3.7. The Mann-Whitney U test indicates no significant differences between MUI on correct and incorrect cases for the two models.

B.6 Impacts of Different Neuron Interpretation Methods

Through utilizing the proposed two explicit interpretation methods, we have unveiled the Utility Law and four corollaries, demonstrating the feasibility of using MUI for model and data evaluation. Moving forward, we will not confine our analysis to a single, fixed neuron or SAEs analysis method. Instead, we aim to employ multiple techniques to ensure a comprehensive and robust analysis, adapting to advancements in the field of interpretability. In this section, we plan to incorporate a broader range of interpretation methods, which will include various definitions of neuron importance (contribution score) and the application of different threshold, to conduct a broad MUI analysis (given that SAE analysis tends to be more static, our exploration for SAE interpretation primarily focus on expanding threshold choices).

B.6.1 Other Neuron Contribution Scores:

Except for projecting activation statistics into the vocabulary, the activation of the inner state can also represent the attribute score of a neuron for predicting \hat{y} given input x . Therefore, following previous work [26], we propose defining the direct use of activation as the contribution score. The contribution of each neuron to the predicted output is calculated as follows:

$$f_{neuron_activation}(i, l, \hat{y} | x) = (\sigma(\mathbf{W}_{in}^l \mathbf{x}_{-1}^l))_{i, \hat{y}} \quad (13)$$

In addition to considering direct activation values, we also explore another definition of neuron importance. Following the work [12], which utilizes Integrated Gradients to define the contribution of each neuron to predictions \hat{y} given input x , we compute this contribution using the following formula:

$$f_{neuron_gradient}(i, l, \hat{y} | x) = \int_{\alpha=0}^1 \partial \left(\alpha (\sigma(\mathbf{W}_{in}^l \mathbf{x}_{-1}^l))_{i, \hat{y}} \right) d\alpha \quad (14)$$

To approximate the integral, we use a Riemann sum approach as described in [12]. This approximation is defined as: $f_{neuron_gradient}(i, l, \hat{y} | x) \approx \frac{1}{m} \sum_{k=1}^m \partial \left(\frac{k}{m} (\sigma(\mathbf{W}_{in}^l \mathbf{x}_{-1}^l))_{i, \hat{y}} \right)$, where m (we deploy $m = 10$) is the number of approximation steps. In addition to using a token-level score, we also explore utilizing a response-level score, which aggregates the scores of each token \hat{y} for each neuron to attribute importance. This method could be implemented based on the prescribed importance calculations from previous equations (Equation 3, Equation 13, Equation 6, and Equation 14).

$$f_{neuron_sum}(i, l, y | x) = \sum_{\hat{y}_j \in y} f_{neuron}(i, l, \hat{y}_j | x + \hat{y}_{<j}) \quad (15)$$

B.6.2 Other Threshold and Selection Standards:

Based on this threshold selection standards in Section 3.8, we test all possible of defined importance measures of neurons, applying various threshold functions with differing threshold value. Our testing methods included: **1)** score-based importance $f_{\text{neuron}}(\text{score})$ as detailed in Equation 3; **2)** activation-based importance $f_{\text{neuron_activation}}(\text{activate})$ as detailed in Equation 13; **3)** gradient-based importance $f_{\text{neuron_gradient}}(\text{gradient})$ as detailed in Equation 14; **4)** response-level score for $f_{\text{neuron}}(\text{score_sum})$; **5)** response-level activation for $f_{\text{neuron_activation}}(\text{activate_sum})$. Each method are tested with a range of threshold functions with specific hyper-parameters: layer-level top-k (topk), global top-k (global_topk), and top-score (topscore). Details on other important measure combinations and threshold selections are provided in bellow:

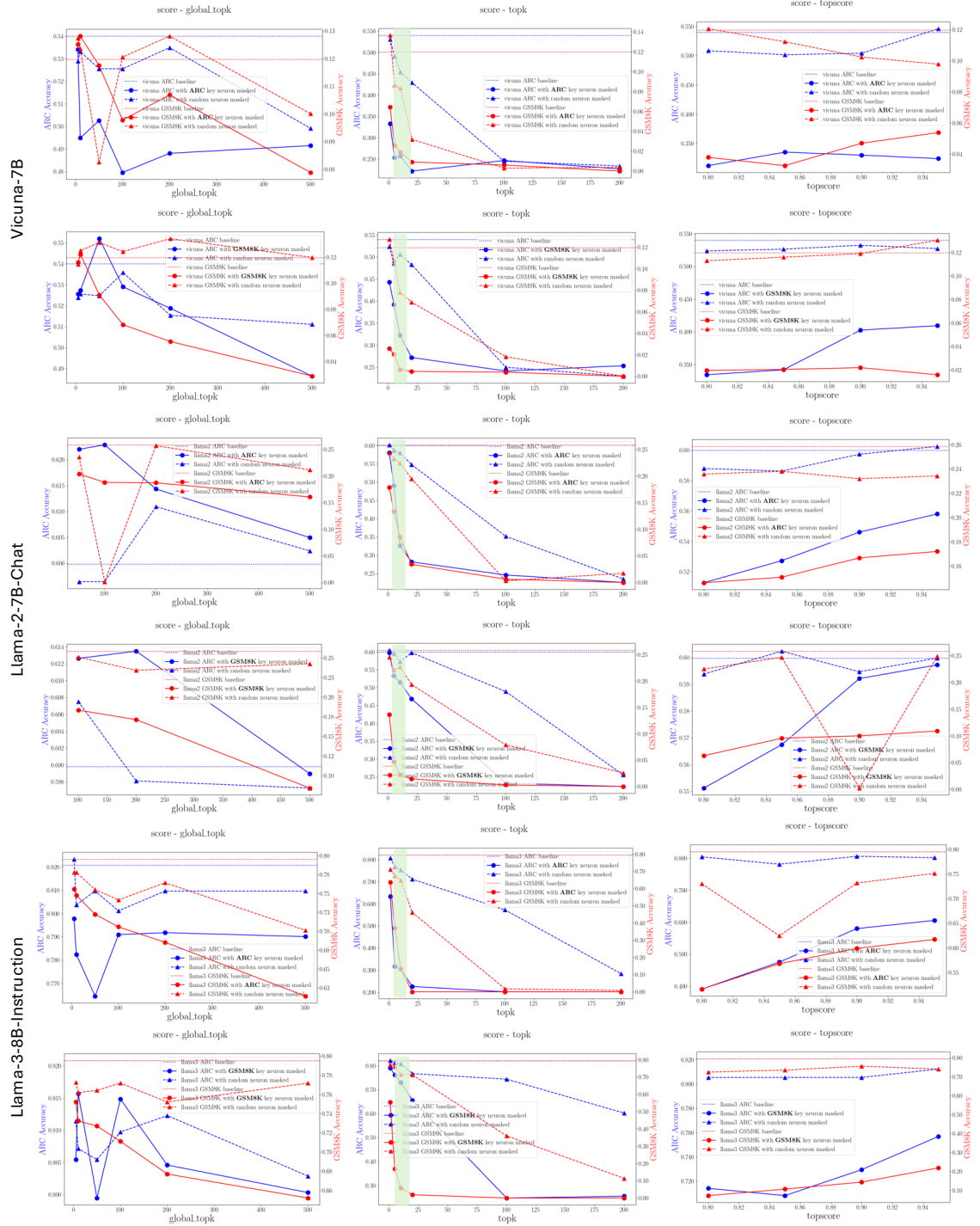


Figure 22: Performance accuracy (accuracy %) of the Vicuna-7B, Llama-2-7B-Chat, Llama-3-8B-Instruction model on the **ARC** and **GSM8K** datasets, with key neurons masked specifically for the **ARC** dataset or the **GSM8K** dataset. Key neurons are identified using a score-based importance measure (see Equation 3) and pre-defined threshold function (Detailed in Appendix A.4). The threshold value used for our MUI analysis —1%, is visually indicated by a green box. The performance impact of masking an equivalent number of key neurons as in the **ARC** / **GSM8K** dataset on the corresponding model is represented with a dashed line.

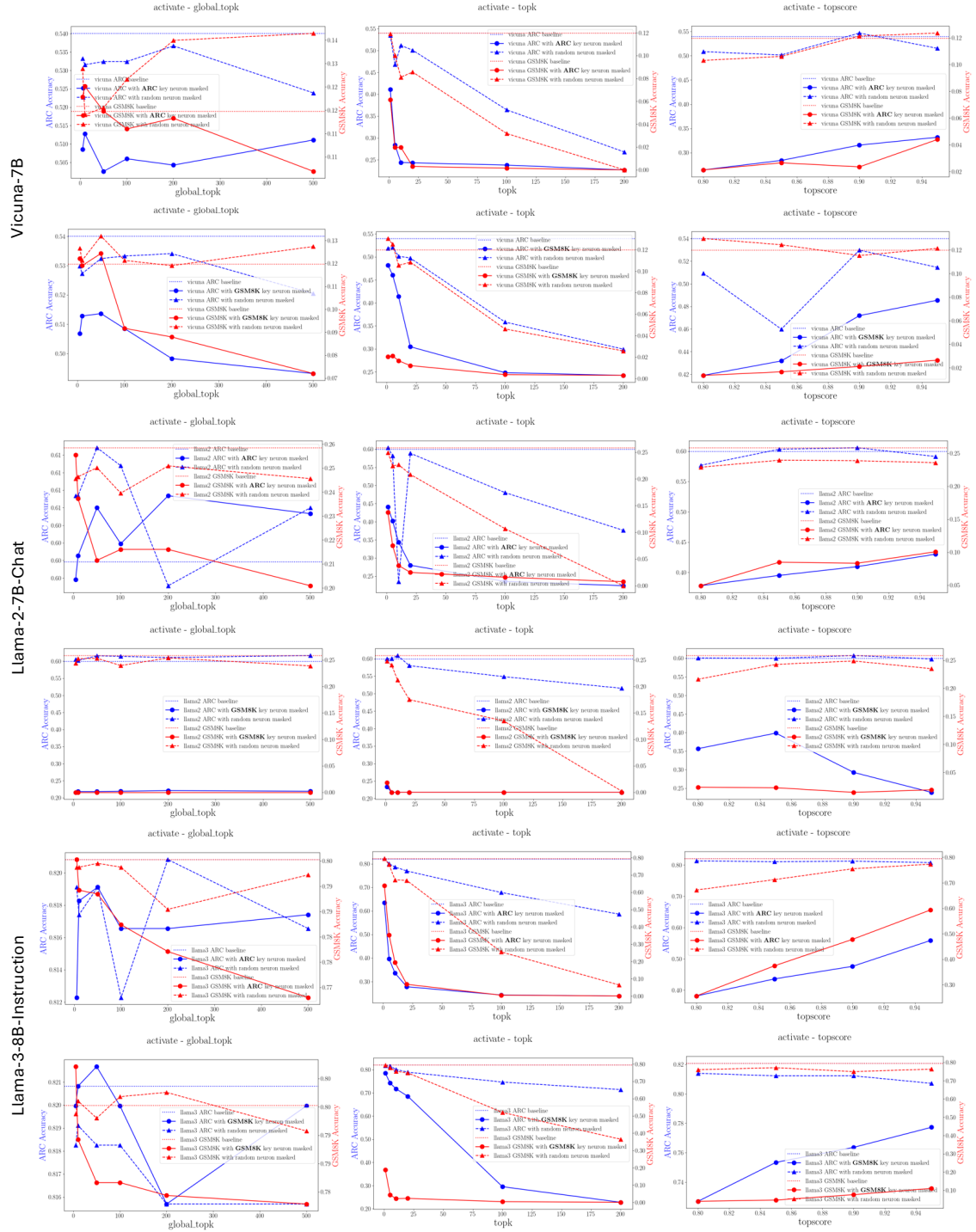


Figure 23: Performance (accuracy %) of the Vicuna-7B, Llama-2-7B-Chat, and Llama-3-8B-Instruction model on the ARC and GSM8K datasets, with key neurons masked specifically for the ARC dataset or the GSM8K dataset. Key neurons are identified using a score-based importance measure (see Equation 13) and pre-defined threshold function (Detailed in Appendix A.4). The performance impact of masking an equivalent number of key neurons as in the ARC / GSM8K dataset on the corresponding model is represented with a dashed line.

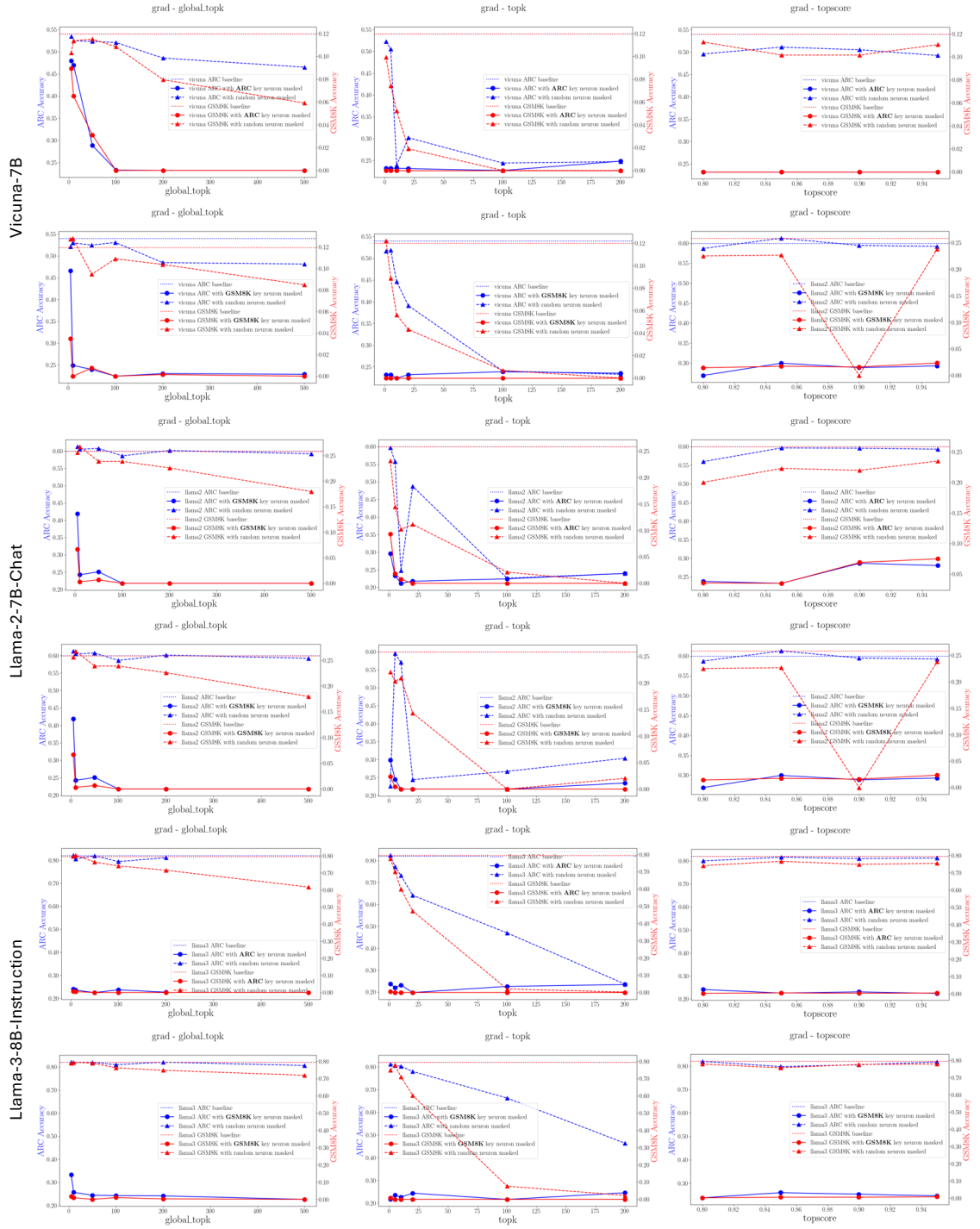


Figure 24: Performance (accuracy %) of the Vicuna-7B, Llama-2-7B-Chat, and Llama-3-8B-Instruction model on the ARC and GSM8K datasets, with key neurons masked specifically for the ARC dataset or the GSM8K dataset. Key neurons are identified using a score-based importance measure (see Equation 14) and pre-defined threshold function (Detailed in Appendix A.4). The performance impact of masking an equivalent number of key neurons as in the ARC / GSM8K dataset on the corresponding model is represented with a dashed line.

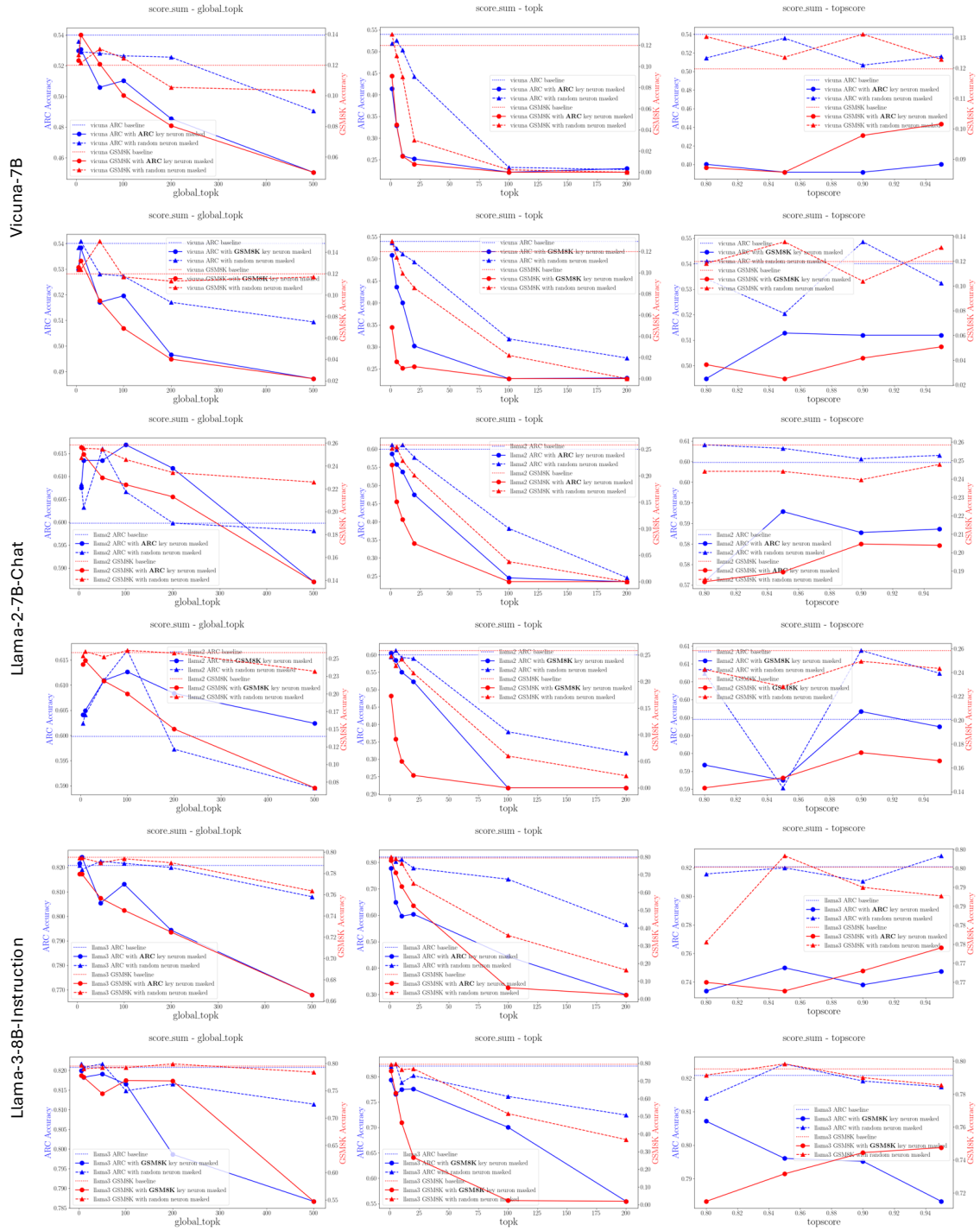


Figure 25: Performance (accuracy %) of the Vicuna-7B, Llama-2-7B-Chat, and Llama-3-8B-Instruction model on the ARC and GSM8K datasets, with key neurons masked specifically for the ARC dataset or the GSM8K dataset. Key neurons are identified using a score-based importance measure (see Equation 15) and pre-defined threshold function (Detailed in Appendix A.4). The performance impact of masking an equivalent number of key neurons as in the ARC / GSM8K dataset on the corresponding model is represented with a dashed line.

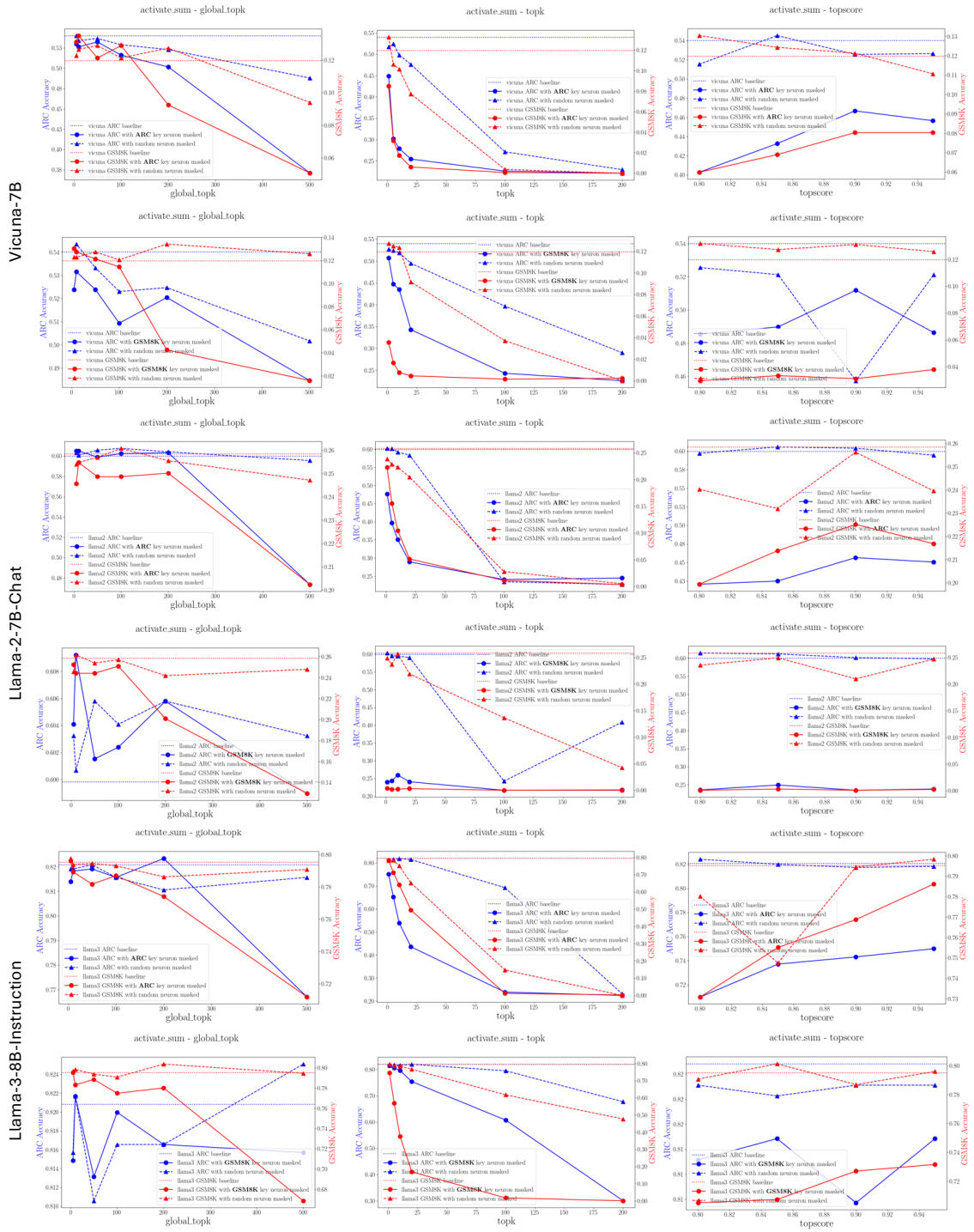


Figure 26: Performance (accuracy %) of the Vicuna-7B, Llama-2-7B-Chat, and Llama-3-8B-Instruction model on the ARC and GSM8K datasets, with key neurons masked specifically for the ARC dataset or the GSM8K dataset. Key neurons are identified using a score-based importance measure (see Equation 15) and pre-defined threshold function (Detailed in Appendix A.4). The performance impact of masking an equivalent number of key neurons as in the ARC / GSM8K dataset on the corresponding model is represented with a dashed line.

B.6.3 Impact of Different Neuron Interpretation Methods

To demonstrate that our analysis is both generalizable and inclusive, we expand to incorporate various interpretation methods. Continuing from our previous threshold selections B.6.3, we conduct analyses using these methods to evaluate changes in the Model Utilization Index (MUI), with a particular focus on the consistency of MUI trends for different model. For some threshold values that do not integrate effectively, we randomly selected a threshold value within the testing range to facilitate a quantitative comparison. The results, which encompass the full parameter range, are detailed in the Figure 27. After applying different interpretation methods, we found that the MUI derived from various approaches (Table 13 and Table 14) correlates well with our experiment selections (Table 11), achieving an average Spearman correlation coefficient of 0.921. This indicates that the overall trend is relatively consistent that model capability and MUI is in a reverse Relationship. However, due to differences in the definition of importance, some models, such as Qwen2.5, exhibit a higher MUI when using activation-based methods compared to Llama3.1.

For SAE interpretation, where feature contribution scores are defined consistently, we considered various thresholds to examine consistency. The results revealed that the selected thresholds (Table 16 and Table 17) align closely with our experimental (Table 15) thresholds, achieving a Spearman correlation coefficient of 0.984. This high correlation demonstrates a strong consistency across different thresholds and confirms the reliability of our SAE interpretation approach in MUI analysis.

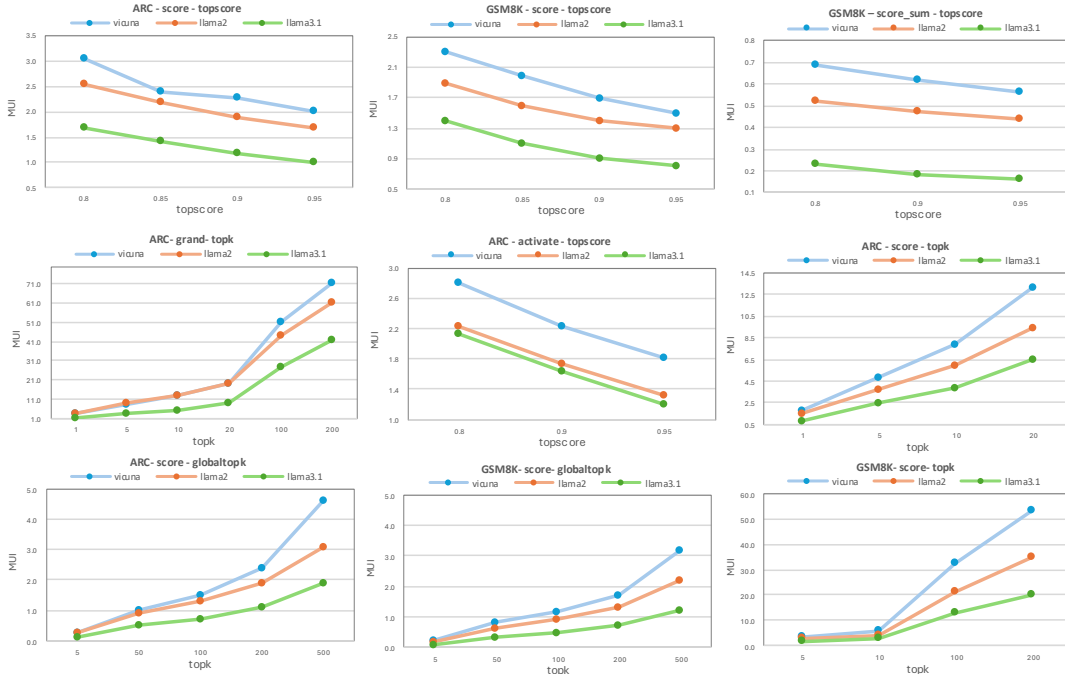


Figure 27: MUI (%) for Vicuna-7B, Llama-2-7B-Chat, and Llama-3-8B-Instruction, across various combinations of neuron importance definitions and threshold. The results demonstrate that the rank order of the three models remains consistent across different interpretation settings.

Model	GSM8K (Math & Reasoning)	MATH (Math & Reasoning)	ARC _c (Math & Reasoning)	HumanEval (Code)	MBPP (Code)	BBH (General)	MLLU (General)
Vicuna-7B	11.9 / 6.0	4.0 / 6.4	54.0 / 8.5	13.4 / 1.3	23.6 / 2.0	28.6 / 8.9	45.3 / 27.4
Llama-2-7B-Chat	25.8 / 4.3	5.4 / 5.5	60.0 / 6.3	16.4 / 1.0	24.8 / 1.7	26.2 / 8.7	48.2 / 17.6
Qwen1.5-7B-Chat	58.7 / 3.7	17.9 / 4.6	76.2 / 7.3	39.0 / 1.3	39.8 / 1.9	41.3 / 9.4	58.3 / 21.3
Llama-3.1-8B-Instruct	86.5 / 3.5	48.1 / 5.0	81.9 / 5.0	62.2 / 1.5	57.9 / 2.7	65.4 / 9.0	64.4 / 18.0
Gemma2-9B-Instruct	82.3 / 2.6	33.5 / 4.3	89.5 / 4.7	63.4 / 0.9	61.2 / 1.5	57.5 / 6.1	73.3 / 14.6
Qwen2.5-7B-Instruct	84.5 / 2.3	61.9 / 3.5	86.8 / 5.4	71.3 / 0.9	62.1 / 1.6	66.0 / 6.6	71.3 / 17.7

Table 11: Performance acc(%) / Activated proportion MUI(%) of the selected model. With score-based importance (Equation 3) and top 1% threshold.

Model	GSM8K (Math & Reasoning)	MATH (Math & Reasoning)	ARC _c (Math & Reasoning)	HumanEval (Code)	MBPP (Code)	BBH (General)	MMLU (General)
Vicuna-7B	11.9 / 7.5	4.0 / 7.9	54.0 / 10.6	13.4 / 1.6	23.6 / 2.5	28.6 / 11.2	45.3 / 33.6
Llama-2-7B-Chat	25.8 / 5.3	5.4 / 6.8	60.0 / 7.7	16.4 / 1.3	24.8 / 2.1	26.2 / 10.9	48.2 / 21.3
Qwen1.5-7B-Chat	58.7 / 4.5	17.9 / 5.6	76.2 / 9.2	39.0 / 1.5	39.8 / 2.4	41.3 / 11.5	58.3 / 25.5
Llama-3.1-8B-Instruct	86.5 / 3.6	48.1 / 5.1	81.9 / 5.3	62.2 / 1.6	57.9 / 2.8	63.4 / 9.4	64.4 / 18.7
Qwen2.5-7B-Instruct	84.5 / 2.0	61.9 / 3.1	86.8 / 4.8	71.3 / 0.8	62.1 / 1.4	61.5 / 6.0	71.3 / 16.0

Table 12: Performance acc(%) / Activated proportion MUI(%) of the selected model. With score-based importance (Equation 3) and topk ($k = 15$) threshold.

Model	GSM8K (Math & Reasoning)	MATH (Math & Reasoning)	ARC _c (Math & Reasoning)	HumanEval (Code)	MBPP (Code)	BBH (General)	MMLU (General)
Vicuna-7B	11.9 / 3.2	4.0 / 3.5	54.0 / 5.0	13.4 / 0.8	23.6 / 1.1	28.6 / 4.7	45.3 / 15.3
Llama-2-7B-Chat	25.8 / 2.5	5.4 / 3.4	60.0 / 3.9	16.4 / 0.7	24.8 / 1.1	26.2 / 5.5	48.2 / 11.2
Qwen1.5-7B-Chat	58.7 / 2.4	17.9 / 2.6	76.2 / 4.4	39.0 / 0.7	39.8 / 1.0	41.3 / 5.6	58.3 / 13.1
Llama-3.1-8B-Instruct	86.5 / 1.7	48.1 / 2.4	81.9 / 2.5	62.2 / 0.8	57.9 / 1.2	63.4 / 4.1	64.4 / 9.1
Qwen2.5-7B-Instruct	84.5 / 2.0	61.9 / 3.5	86.8 / 4.8	71.3 / 0.9	62.1 / 1.6	61.5 / 6.0	71.3 / 19.6

Table 13: Performance acc(%) / Activated proportion MUI(%) of the selected model. With activation-based importance (Equation 13) and topk ($k = 10$) threshold.

Model	GSM8K (Math & Reasoning)	MATH (Math & Reasoning)	ARC _c (Math & Reasoning)	HumanEval (Code)	MBPP (Code)	BBH (General)	MMLU (General)
Vicuna-7B	11.9 / 2.4	4.0 / 3.7	54.0 / 3.4	13.4 / 0.6	23.6 / 1.0	28.6 / 3.5	45.3 / 13.6
Llama-2-7B-Chat	25.8 / 2.4	5.4 / 4.4	60.0 / 3.6	16.4 / 0.6	24.8 / 0.8	26.2 / 3.8	48.2 / 15.4
Qwen1.5-7B-Chat	58.7 / 1.9	17.9 / 3.5	76.2 / 2.6	39.0 / 0.4	39.8 / 0.8	41.3 / 3.7	58.3 / 10.1
Llama-3.1-8B-Instruct	86.5 / 0.9	48.1 / 2.0	81.9 / 1.2	62.2 / 0.3	57.9 / 0.6	63.4 / 2.9	64.4 / 6.5
Qwen2.5-7B-Instruct	84.5 / 1.8	61.9 / 4.0	86.8 / 2.8	71.3 / 0.4	62.1 / 0.8	61.5 / 3.8	71.3 / 14.0

Table 14: Performance acc(%) / Activated proportion MUI(%) of the selected model. With gradient-based importance (Equation 14) and top score ($k = 0.95$) as the threshold.

Model	GSM8K (Math & Reasoning)	MATH (Math & Reasoning)	ARC _c (Math & Reasoning)	HumanEval (Code)	MBPP (Code)	BBH (General)	MMLU (General)
Llama-3.1-8B	42.9 / 1.9	15.1 / 2.0	77.1 / 3.2	19.5 / 0.40	26.1 / 0.7	50.1 / 3.9	59.6 / 13.0
Gemma2-9B	65.8 / 1.7	20.8 / 2.4	84.6 / 3.2	54.8 / 0.37	57.7 / 0.5	67.4 / 2.2	67.2 / 9.6

Table 15: Performance (accuracy %) under one-shot inference setting / SAE-based Model Utilization Index (MUI) (%) of the selected model. With topk ($k = 50$) as the threshold.

Model	GSM8K (Math & Reasoning)	MATH (Math & Reasoning)	ARC _c (Math & Reasoning)	HumanEval (Code)	MBPP (Code)	BBH (General)	MMLU (General)
Llama-3.1-8B	42.9 / 0.6	15.1 / 0.7	77.1 / 1.0	19.5 / 0.10	26.1 / 0.2	50.1 / 1.4	59.6 / 5.6
Gemma2-9B	65.8 / 0.5	20.8 / 0.7	84.6 / 0.9	54.8 / 0.08	57.7 / 0.1	67.4 / 0.7	67.2 / 4.8

Table 16: Performance (accuracy %) under one-shot inference setting / SAE-based Model Utilization Index (MUI) (%) of the selected model. With topk ($k = 10$) as the threshold.

Model	GSM8K (Math & Reasoning)	MATH (Math & Reasoning)	ARC _c (Math & Reasoning)	HumanEval (Code)	MBPP (Code)	BBH (General)	MMLU (General)
Llama-3.1-8B	42.9 / 0.24	15.1 / 0.31	77.1 / 0.44	19.5 / 0.05	26.1 / 0.09	50.1 / 0.62	59.6 / 2.89
Gemma2-9B	65.8 / 0.21	20.8 / 0.32	84.6 / 0.40	54.8 / 0.03	57.7 / 0.04	67.4 / 0.31	67.2 / 1.79

Table 17: Performance (accuracy %) under one-shot inference setting / SAE-based Model Utilization Index (MUI) (%) of the selected model. With top score ($k = 0.9$) as the threshold.

C Few-shot Instruction

ARC:

Question: A comet passes close to a planet, causing a slight wobble in its orbit. Which is the most likely effect of this wobble?

- A. The planet will move faster in its orbit.
- B. The planet's orbit will become more elliptical.
- C. The planet's axial tilt will change.
- D. The planet's temperature will increase.

Answer: The correct answer is C. The planet's axial tilt will change. The wobble in the orbit, also known as "axial precession," can alter the angle at which the planet tilts on its axis, affecting its seasons and climate.

GSM8K:

Question: Weng earns \$12 an hour for babysitting. Yesterday, she just did 50 minutes of babysitting. How much did she earn?

Answer: Weng babysat for 50 minutes, which is $\frac{50}{60} = \frac{5}{6}$ of an hour. At \$12 per hour, her earnings are:

$$12 \times \frac{5}{6} = 10 \text{ dollars.}$$

So the answer is \$10.

HumanEval & MBPP:

Question: Write a Python function `alternate(numbers: List[int], value: int) -> List[int]` to solve the following problem: Alternate between the elements of the input list `numbers` and the value. The value should appear between every two consecutive elements of `numbers`, and at the beginning and end.

```
1 >>> alternate([], 5)
2 []
3 >>> alternate([1, 2, 3], 5)
4 [5, 1, 5, 2, 5, 3, 5]
```

Answer: To implement the `alternate` function, we can iterate through the list and insert the value between each element of the list, as well as at the beginning and end of the list. Here's how you can do it:

```
1 from typing import List
2
3 def alternate(numbers: List[int], value: int) -> List[int]:
4     """Alternate between the elements of the input list 'numbers
5         ↳ and the 'value'.
6     """
7     >>> alternate([], 5)
8     []
9     >>> alternate([1, 2, 3], 5)
10    [5, 1, 5, 2, 5, 3, 5]
11    """
12    if not numbers: # If the list is empty, return an empty
13        ↳ list
14        return []
15
16    result = [value] # Start with the value at the beginning
17    for num in numbers:
18        result.append(num)
19        result.append(value) # Add value after each number
20    return result
```


MATH:

Problem: Find $\tan 45^\circ$.

Solution: We know that $\tan 45^\circ = \frac{\sin 45^\circ}{\cos 45^\circ}$. Since $\sin 45^\circ$ and $\cos 45^\circ$ are both equal to $\frac{\sqrt{2}}{2}$, it follows that:

$$\tan 45^\circ = \frac{\sin 45^\circ}{\cos 45^\circ} = \frac{\frac{\sqrt{2}}{2}}{\frac{\sqrt{2}}{2}} = 1.$$

Therefore, the solution is 1.

MMLU:

Question: Where is the sinoatrial node located?

- A. Between the left atrium and the left ventricle
- B. Between the right atrium and the right ventricle
- C. In the upper wall of the right atrium
- D. In the upper wall of the left ventricle

Answer: The correct answer is C.

Here's why: The sinoatrial (SA) node is the heart's natural pacemaker. It's responsible for initiating the electrical impulses that cause the heart to contract and pump blood. Its location in the right atrium allows it to efficiently send these impulses throughout the heart.